CrossMark
click for updates

View Article Online
View Journal

Dalton Transactions

Accepted Manuscript

This article can be cited before page numbers have been issued, to do this please use: F. He, L. RUHLMANN, J. Gisselbrecht, S. Choua, M. Orio, M. Wesolek, A. Danopoulos and P. Braunstein, *Dalton Trans.*, 2015, DOI: 10.1039/C5DT02403J.

This is an *Accepted Manuscript*, which has been through the Royal Society of Chemistry peer review process and has been accepted for publication.

Accepted Manuscripts are published online shortly after acceptance, before technical editing, formatting and proof reading. Using this free service, authors can make their results available to the community, in citable form, before we publish the edited article. We will replace this *Accepted Manuscript* with the edited and formatted *Advance Article* as soon as it is available.

You can find more information about *Accepted Manuscripts* in the Information for Authors.

Please note that technical editing may introduce minor changes to the text and/or graphics, which may alter content. The journal's standard Terms & Conditions and the Ethical guidelines still apply. In no event shall the Royal Society of Chemistry be held responsible for any errors or omissions in this *Accepted Manuscript* or any consequences arising from the use of any information it contains.

ROYAL SOCIETY OF CHEMISTRY

www.rsc.org/dalton

View Article Online
DOI: 10.1039/C5DT02403J

Journal Name

ARTICLE

Dinuclear Iridium and Rhodium Complexes with Bridging Arylimidazolide-N^3,C^2 Ligands: Synthetic, Structural, Reactivity, Electrochemical and Spectroscopic Studies†

Received 00th January 20xx,
Accepted 00th January 20xx

DOI: 10.1039/x0xx00000x

www.rsc.org/

Dinuclear Iridium and Rhodium Complexes with Bridging Arylimidazolide-N^3,C^2 Ligands: Synthetic, Structural, Reactivity, Electrochemical and Spectroscopic Studies†

Fan He,[a] Laurent Ruhlmann,[b] Jean-Paul Gisselbrecht,[b] Sylvie Choua,[c] Maylis Orio,[e] Marcel Wesolek,[a] Andreas A. Danopoulos,*[a,d] Pierre Braunstein*[a]

Deprotonation of 1-arylimidazoles (aryl = mesityl (Mes), 2,6-diisopropylphenyl (Dipp)), with *n*-butyl lithium afforded the corresponding derivatives (1-aryl-1*H*-imidazol-2-yl)lithium (**1a**, Ar = Mes; **1b**, Ar = Dipp) in good yield. Reaction of **1a** with 0.5 equiv. of $[Ir(cod)(\mu\text{-}Cl)]_2$ yielded two geometrical isomers of a doubly C2,N3-bridged dinuclear complex $[Ir(cod)\{\mu\text{-}C_3H_2N_2(Mes)\text{-}\kappa C2,\kappa N3\}]_2$ (**3**), $\mathbf{3_{H\text{-}H}}$, a head-to-head (H-H) isomer of C_s symmetry, and $\mathbf{3_{H\text{-}T}}$, the thermodynamically preferred head-to-tail (H-T) isomer of C_2 symmetry. The metallated carbon of the 4 electron donor anionic bridging ligands has some carbene character, reminiscent of the situation in N-metallated protic NHC complexes. Displacement of cod ligands from $\mathbf{3_{H\text{-}H}}$ and $\mathbf{3_{H\text{-}T}}$ afforded the tetracarbonyl complexes $[Ir(CO)_2\{\mu\text{-}C_3H_2N_2(Mes)\text{-}\kappa C2,\kappa N3\}]_2$ $\mathbf{4_{H\text{-}H}}$ and $\mathbf{4_{H\text{-}T}}$, respectively. The reaction with PMe_3, which gave only one complex, $[Ir(CO)(PMe_3)\{\mu\text{-}C_3H_2N_2(Mes)\text{-}\kappa C2,\kappa N3\}]_2$ (**5**), demonstrates that the isomerization of the central core $Ir[\mu\text{-}C_3H_2N_2(Mes)\text{-}\kappa C2,\kappa N3]_2Ir$ from H-H to H-T on going from $\mathbf{4_{H\text{-}H}}$ to **5** is readily triggered by phosphine substitution under mild conditions. Oxidative-addition of MeI to **5** afforded the formally metal-metal bonded d^7-d^7 complex $[Ir_2(CO)_2(PMe_3)_2(Me)I\{\mu\text{-}C_3H_2N_2(Mes)\text{-}\kappa C2,\kappa N3\}_2]$ (**6**). The blue $[Ir(C_2H_4)_2\{\mu\text{-}C_3H_2N_2(Mes)\text{-}\kappa C2,\kappa N3\}]_2$ (**7**) and purple $[Rh(C_2H_4)_2\{\mu\text{-}C_3H_2N_2(Dipp)\text{-}\kappa C2,\kappa N3\}]_2$ (**9**) tetraethylene complexes were also obtained with only a H-T arrangement of the bridging ligands. Although only modestly efficient in alkane dehydrogenation, complex **7** was found to be a more active pre-catalyst than $\mathbf{3_{H\text{-}T}}$, $\mathbf{4_{H\text{-}T}}$ and **5**, probably because of the favorable lability of the ethylene ligands. From cyclic voltammetry, exhaustive coulometry and spectroelectrochemistry studies, it was concluded that $\mathbf{3_{H\text{-}T}}$ undergoes a metal-based one electron oxidation to generate the mixed-valent Ir(I)/Ir(II) system. The energy of the intervalence band for the orange dirhodium complex $[Rh(cod)\{\mu\text{-}C_3H_2N_2(Mes)\text{-}\kappa C2,\kappa N3\}]_2$ (**8**) is shifted toward lower energies in comparison with $\mathbf{3_{H\text{-}T}}$, reflecting the decrease of the energy with the intermetallic distance. It was concluded from the EPR study that the Ir and Rh centres contribute substantially to the experimental magnetic anisotropy and thus to the singly occupied molecular orbital (SOMO) in the mixed-valent Ir(I)/Ir(II) and Rh(I)/Rh(II) systems. The molecular structures of $\mathbf{3_{H\text{-}H}}$, $\mathbf{3_{H\text{-}T}}$, **8** and **9** have

[a] *Laboratoire de Chimie de Coordination, Institut de Chimie (UMR 7177 CNRS), Université de Strasbourg, 4 rue Blaise Pascal, 67081 Strasbourg Cedex (France). E-mail: braunstein@unistra.fr*
[b] *Laboratoire d'Electrochimie et de Chimie Physique du Corps Solide, Institut de Chimie (UMR 7177 CNRS), Université de Strasbourg, 4 rue Blaise Pascal, 67081 Strasbourg Cedex (France). E-mail: danopoulos@unistra.fr*
[c] *Institut de Chimie, Université de Strasbourg, 1 rue Blaise Pascal, BP 296 R8, F-67008 Strasbourg, Cedex (France).*
[d] *Université de Strasbourg, Institute for Advanced Study (USIAS), Strasbourg (France).*
[e] *Institut des Sciences Moléculaires de Marseille, Aix Marseille Université, CNRS, Centrale Marseille, ISM2 UMR 7313, 13397, Marseille, France*

† Electronic Supplementary Information (ESI) available: Table S1 containing the crystal data for $\mathbf{3_{H\text{-}H}}$, $\mathbf{3_{H\text{-}T}}$, **8** and **9** (CCDC 1052655–1052658), figures showing UV-visible-NIR spectra (S1, S3), ^{1}H NMR spectra (S2, S4), cyclic voltammograms (S5–S7), time-resolved UV-visible-NIR absorption spectra (S8, S9), EPR spectra (S10), the optimized structures (S11, S13), spin population distribution and SOMO (S12, S14). For ESI and crystallographic data in CIF format see DOI: 10.1039/x0xx00000x

Published on 23 July 2015. Downloaded by University of California - Santa Barbara on 28/07/2015 05:09:18.

Dalton Transactions Accepted Manuscript

View Article Online
DOI: 10.1039/C5DT02403J

Published on 23 July 2015. Downloaded by University of California - Santa Barbara on 28/07/2015 05:09:18.

been determined by X-ray diffraction.

Introduction

The isolation by Arduengo and co-workers of stable N-heterocyclic carbenes (NHCs) of the imidazole type with bulky *N*-substituents,[1] has triggered a fast growing interest for this class of ligands, in particular in organometallic chemistry.[2] Protic NHCs (pNHCs) are characterised by the presence of a N-bound H atom and have been comparatively much less investigated, despite their strong σ-donor character and the possibility for the *N*H group to be involved in secondary interactions of potential relevance to bifunctional catalysis,[3] substrate recognition[4] and biological systems.[5]

Different synthetic methodologies allow access to pNHC metal complexes: building the C-bound heterocycle in the metal coordination sphere,[6] using suitable N-protecting groups that are removed after metal coordination,[7] or facilitating the kinetic formation of the M–C_{NHC} bond by the oxidative-addition of the C–X bond of halo-imidazoles (X = halide).[8] Most recently, we found that *N*-arylimine-functionalized pNHC Ir(I) and Ir(III) complexes could be readily obtained from cationic or neutral Ir(I) imidazole complexes using excess $TlPF_6$ or $[Ir(cod)(\mu\text{-}Cl)]_2$, respectively.[9] Deprotonation of such a pNHC Ir(I) complex was shown to give rise to an equilibrium between a mononuclear complex containing a C-bound 'anionic' imidazolide and its dimer in which this moiety binds in a μ-C,N bridging mode (Scheme 1).[9]

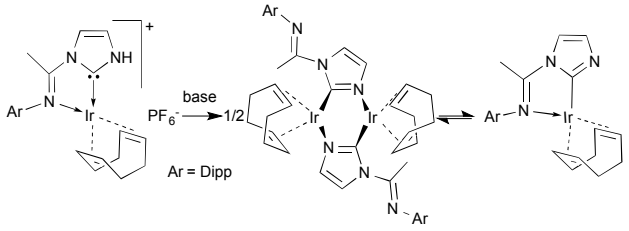

Scheme 1 Deprotonation of a protic NHC (pNHC) Ir(I) complex leading to an equilibrium between a mononuclear complex containing a C-bound 'anionic' imidazolide and its dimer.[9]

Anionic imidazolides possess interesting properties. Lithium 1-methyl-(4-*t*-butyl)imidazolide was found by Boche and co-workers to have carbene character, as supported by the ^{13}C NMR chemical shift of its C2 atom (δ 195.9) and an X-ray diffraction study.[10] Kostyuk and co-workers reported a method to synthesize N-phosphorylated carbenes by the reaction between lithium imidazolides, bearing a bulky N-bound *t*-butyl or adamantyl group, and di(*t*-butyl)chlorophosphine.[11] Furthermore, an imidazolide can act as a N,C-bidentate ligand, comparable to a pyrazolide. While dinuclear bis(μ-pyrazolido)iridium(I) complexes have been widely investigated in oxidative addition reactions,[12] substitution chemistry,[13] kinetic[14] and theoretical studies,[15] no extensive study on dinuclear iridium complexes bearing imidazolides has yet been carried out.[16] A brief report described in 1983 the synthesis of dinuclear imidazolide Rh(I) complexes by deprotonation with MeLi of a mononuclear imidazole complex.[17] As part of our current investigations on the tautomerism/metallotropism between pNHC and imidazole ligands in iridium complexes (Scheme 2),[9] we describe herein the synthesis, structural and spectroscopic characterisation, reactivity and electrochemical properties of a series of doubly C,N-bridged dinuclear iridium and rhodium complexes bearing 1-arylimidazolide ligands.

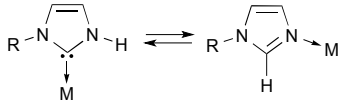

Scheme 2 Tautomerism/metallotropism between pNHC and imidazole ligands.[9]

Results and discussion

Synthesis and characterisation of the di-iridium complexes.

Starting from 1-arylimidazoles (aryl = mesityl (Mes), 2,6-diisopropylphenyl (Dipp)), the corresponding derivatives (1-aryl-1*H*-imidazol-2-yl)lithium (1a, Ar = Mes; 1b, Ar = Dipp) were prepared in good yield by deprotonation with a stoichiometric amount of *n*-butyl lithium in pentane at -30 °C (Scheme 3).

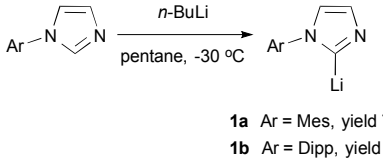

Scheme 3 Synthesis of (1-aryl-1*H*-imidazol-2-yl)lithium (**1a,b**).

In their NMR spectra in THF-d_8, the absence of the ^1H NMR resonance of the proton at C2 and the values of $^{13}C\{^1H\}$ NMR resonance due to the C2 carbon, at δ 205.8 for (1-mesityl-1*H*-imidazol-2-yl)lithium (**1a**) and δ 202.3 for (1-(2,6-diisopropyl phenyl)-1*H*-imidazol-2-yl)lithium (**1b**), consistent with the metallation of this carbon.

Dalton Transactions Accepted Manuscript

View Article Online
DOI: 10.1039/C5DT02403J

Published on 23 July 2015. Downloaded by University of California - Santa Barbara on 28/07/2015 05:09:18.

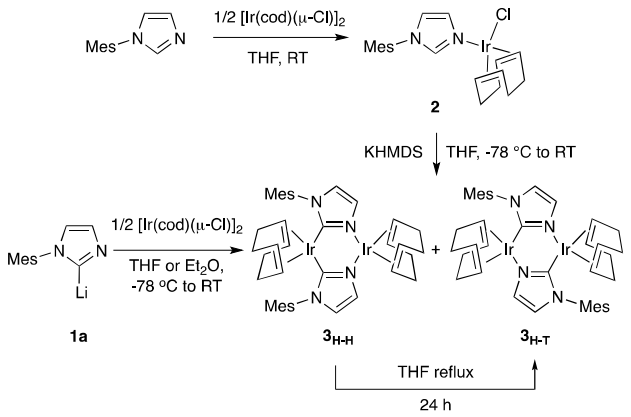

Scheme 4 Stepwise or direct synthesis of the two isomers of the dinuclear complexes $\mathbf{3_{H\text{-}H}}$ and $\mathbf{3_{H\text{-}T}}$.

Treatment of **1a** with 0.5 equiv. of $[Ir(cod)(\mu\text{-}Cl)]_2$ at -78 °C in THF led to the formation of the doubly C,N-bridged dinuclear complex $[Ir(cod)\{\mu\text{-}C_3H_2N_2(Mes)\text{-}\kappa C2,\kappa N3\}]_2$ (**3**) as a red solid in nearly quantitative yield (Scheme 4). Its ^1H and $^{13}C\{^1H\}$ NMR spectra in C_6D_6 revealed the presence of a *ca.* 40:60 mixture of two constitutional isomers, $\mathbf{3_{H\text{-}H}}$, a head-to-head isomer of C_S symmetry, and $\mathbf{3_{H\text{-}T}}$, a head-to-tail isomer of C_2 symmetry. In the NMR spectra of the mixture in C_6D_6, each isomer displays one set of mesityl, imidazolide and cod signals. The chemical shifts of the $^{13}C\{^1H\}$ NMR resonance due to the C2 carbon (δ 171.3 and 172.0) are considerably upfield-shifted when compared to the value of 205.8 ppm in **1a**. It turned out to be difficult to efficiently separate and isolate each isomer pure out of this mixture because of their similar solubilities. Another procedure to prepare doubly C,N-bridged dinuclear complexes was found to consist of the deprotonation of 1-mesitylimidazolyl(cycloocta-1,5-diene) iridium(I) chloride $[Ir(cod)Cl\{C_3H_3N_2(Mes)\text{-}\kappa N3\}]$ (**2**) with a stoichiometric amount of potassium bis(trimethylsilyl)amide (KHMDS) in THF at -78 °C. According to the NMR spectra, a *ca.* 40:60 mixture of the same two isomers $\mathbf{3_{H\text{-}H}}$ and $\mathbf{3_{H\text{-}T}}$ was again obtained. However, when the reaction using **1a** was repeated in Et_2O,[16b] the resulting red suspension was found to consist of a *ca.* 90:10 mixture of $\mathbf{3_{H\text{-}H}}$ and $\mathbf{3_{H\text{-}T}}$, after dissolution in toluene and ^1H NMR analysis. This difference in proportions obtained in THF is likely due to the lower solubility of $\mathbf{3_{H\text{-}H}}$ in Et_2O. After recrystallization from a toluene/ Et_2O solution at -30 °C, deep red crystals of one pure isomer were obtained in 80% yield. In its ^1H NMR spectrum (C_6D_6), the C4 and C5 imidazolyl protons gave rise to an AX pattern at δ 7.20 (d) and 6.42 (d, ^3J = 1.4 Hz). In the $^{13}C\{^1H\}$ NMR spectrum, the three resonances at δ 171.3, 125.5 and 122.4 are assigned to the C2, C4 and C5 imidazolyl carbons, respectively. However, a definitive assignment of this isomer as H-H or H-T was impossible on the exclusive basis of the spectroscopic data. Fortunately, its structure was elucidated by X-ray diffraction analysis and established its H-H arrangement. The molecular structure of $\mathbf{3_{H\text{-}H}}$ is shown in Fig. 1, with selected bond lengths and angles. The C_s molecular symmetry of the complex in solution is almost retained in the solid state, as indicated by NMR spectroscopy. The boat conformation of $\mathbf{3_{H\text{-}H}}$ is similar to that of the analogous bridged pyrazolido complex.[12b] There is no direct iridium-iridium interaction since the separation between the metal atoms is 3.1844(9) Å. The iridium(I) centres adopt an approximate square planar coordination geometry, defined by two olefinic bonds of the 1,5-cyclooctadiene ligand and two carbon atoms (or two nitrogen atoms) from the imidazolide bridging ligands. The latter can be formally considered as 4 electron anionic donors toward Ir(I) centres. The electronic environment at the metals is unsymmetrical and Ir(1) is more electron-rich than Ir(2) since it is bound to two carbanionic donors. This is also supported by the difference in redox potentials between the isomers $\mathbf{3_{H\text{-}H}}$ and $\mathbf{3_{H\text{-}T}}$ (Table 1) although in the case of $\mathbf{3_{H\text{-}H}}$ the redox waves are irreversible. The C1–N1 [1.35(2) Å] and C21–N3 [1.35(2) Å] bond lengths are not significantly shorter (within 3σ) than those of C1–N2 [1.38(2) Å] and C21–N4 [1.39(2) Å]. This is indicative of electronic delocalization between the N1, C1 and N2 atoms (N3, C21 and N4, respectively) and of a carbene character for C1 and C21, respectively (Scheme 5).

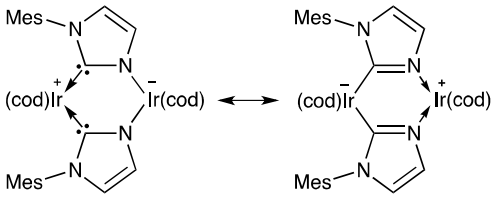

Scheme 5 Limiting resonance structures for the diiridium(I) complex $\mathbf{3_{H\text{-}H}}$ emphasising the dipolar nature of this isomer.

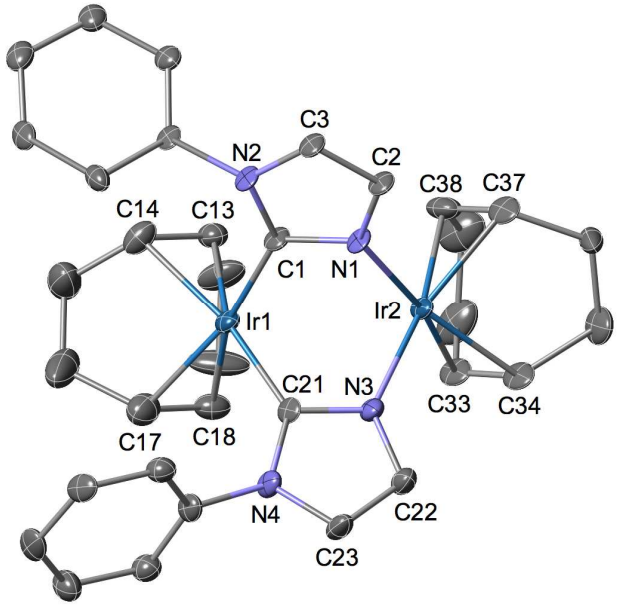

Fig. 1 View of the molecular structure of $\mathbf{3_{H\text{-}H}}$, H atoms and methyl groups are omitted for clarity. Thermal ellipsoids are at the 30% level. Selected bond lengths (Å) and angles (°): Ir1···Ir2 3.1844(9), C1–N1 1.35(2), C1–N2 1.38(2), Ir1–C1 2.05(1), Ir1–C21 2.05(1), Ir1–C13 2.14(1), Ir1–C14 2.18(1), Ir1–C17 2.17(2), Ir1–C18 2.16(2), C13–C14 1.38(2), C17–C18 1.36(3), C21–N3 1.35(2), C21–N4 1.39(2), Ir2–N1 2.07(1), Ir2–N3 2.06(1), Ir2–C33 2.10(1),

Dalton Transactions Accepted Manuscript

View Article Online
DOI: 10.1039/C5DT02403J

Published on 23 July 2015. Downloaded by University of California - Santa Barbara on 28/07/2015 05:09:18.

Ir2–C34 2.09(1), Ir2–C37 2.11(2), Ir2–C38 2.10(2), C33–C34 1.39(3), C37–C38 1.40(3); N1–C1–N2 106(1), N3–C21–N4 105(1), C1–Ir1–C21 87.4(6), C13–Ir1–C14 37.2(6), C14–Ir1–C17 80.6(7), C17–Ir1–C18 36.5(7), C18–Ir1–C13 81.4(6), N1–Ir2–N3 86.5(5), C33–Ir2–C34 38.7(7), C34–Ir2–C37 82.8(6), C37–Ir2–C38 38.7(7), C38–Ir2–C33 81.3(7).

The complex $\mathbf{3_{H\text{-}H}}$ can be thermally converted to its isomer $\mathbf{3_{H\text{-}T}}$ upon refluxing a THF solution for 24 h (Scheme 4). In the ^{1}H NMR spectrum of $\mathbf{3_{H\text{-}T}}$ in C_6D_6, the protons at the imidazolide backbone carbons C4 and C5 give rise to an AX pattern at δ 7.02 (d) and 6.09 (d, ^3J = 1.6 Hz). In the $^{13}C\{^1H\}$ NMR spectrum, the resonances at δ 125.4 and 121.3 are assigned to C4 and C5, respectively. The $^{13}C\{^1H\}$ NMR resonance of the imidazolide C2 carbon (C1 and C21 in Fig. 2) in $\mathbf{3_{H\text{-}T}}$ (δ 172.0) is downfield shifted compared to that in $\mathbf{3_{H\text{-}H}}$ (δ 171.3) (C1 and C21 in Fig. 1). The UV-visible-NIR absorption spectrum of $\mathbf{3_{H\text{-}T}}$ in CH_2Cl_2 is shown in Fig. S1 (see ESI). Single crystals of $\mathbf{3_{H\text{-}T}}$ suitable for X-ray diffraction were obtained by slow diffusion of a layer of Et_2O into a THF solution of $\mathbf{3_{H\text{-}T}}$ at room temperature under argon. The molecular structure of $\mathbf{3_{H\text{-}T}}$ is shown in Fig. 2, with selected bond lengths and angles.

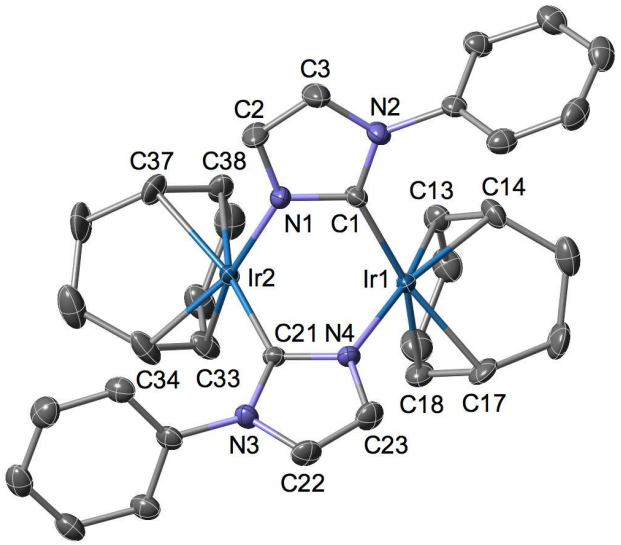

Fig. 2 View of the molecular structure of $\mathbf{3_{H\text{-}T}}$, H atoms and methyl groups are omitted for clarity. Thermal ellipsoids are at the 30% level. Selected bond lengths (Å) and angles (°): Ir1···Ir2 3.1407(2), C1–N1 1.349(5), C1–N2 1.373(5), Ir1–C1 2.058(4), Ir1–N4 2.068(3), Ir1–C13 2.121(4), Ir1–C14 2.112(4), Ir1–C17 2.166(4), Ir1–C18 2.158(4), C13–C14 1.409(6), C17–C18 1.390(6), C21–N3 1.378(5), C21–N4 1.335(5), Ir2–N1 2.067(3), Ir2–C21 2.043(4), Ir2–C33 2.135(4), Ir2–C34 2.118(4), Ir2–C37 2.168(4), Ir2–C38 2.159(4), C33–C34 1.404(7), C37–C38 1.395(6); N1–C1–N2 106.1(3), N3–C21–N4 106.7(3), C1–Ir1–N4 86.9(1), C13–Ir1–C14 38.9(2), C14–Ir1–C17 82.0(2), C17–Ir1–C18 37.5(2), C18–Ir1–C13 81.2(2), N1–Ir2–C21 86.6(1), C33–Ir2–C34 38.6(2), C34–Ir2–C37 82.0(2), C37–Ir2–C38 37.6(2), C38–Ir2–C33 81.2(2).

A boat conformation is observed for the structure of $\mathbf{3_{H\text{-}T}}$, similar to that of its isomer $\mathbf{3_{H\text{-}H}}$. The distance between two iridium atoms (3.1407(2) Å) is shorter than in $\mathbf{3_{H\text{-}H}}$ but still too long to represent a direct metal-metal interaction. Each iridium atom has a 16 valence electron configuration and adopts an approximate square planar coordination geometry, defined by two olefinic bonds of the 1,5-cyclooctadiene ligand, one carbon atom of one imidazolide and one nitrogen atom of the other bridging imidazolide ligand. The C1–N1 and C21–N4 distances of 1.349(5) Å and 1.335(5) Å, respectively, are almost identical to the corresponding distances in $\mathbf{3_{H\text{-}H}}$ (1.35(2) Å). A similar comment applies to the bond lengths C1–N2 1.373(5) and C21–N3 1.378(5) which compare with the corresponding values of 1.38(2) and 1.39(2) Å in $\mathbf{3_{H\text{-}H}}$. This, together with the similarity between the C-N bond lengths in $\mathbf{3_{H\text{-}T}}$, is consistent with the resonance structures shown in Scheme 6.

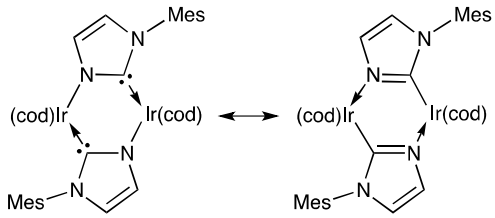

Scheme 6 Limiting resonance structures for $\mathbf{3_{H\text{-}T}}$..

Displacement Reactions of the cod Ligands.

With the original aim to prepare derivatives of $\mathbf{3_{H\text{-}H}}$ and $\mathbf{3_{H\text{-}T}}$ in which replacement of the cod ligands with two-electron donor ligands could modify the redox properties, as monitored by cyclic voltammetry, the tetracarbonyl derivatives $[Ir(CO)_2\{\mu\text{-}C_3H_2N_2(Mes)\text{-}\kappa C2,\kappa N3\}]_2$ ($\mathbf{4_{H\text{-}H}}$ and $\mathbf{4_{H\text{-}T}}$, respectively) were readily synthesized by reaction with carbon monoxide in Et_2O (Scheme 7). While a clear brown Et_2O solution of $\mathbf{4_{H\text{-}T}}$ was obtained, the reaction with $\mathbf{3_{H\text{-}H}}$ led to a yellow suspension. The higher solubility of $\mathbf{4_{H\text{-}T}}$ in Et_2O compared to that of $\mathbf{4_{H\text{-}H}}$ is consistent with their different polarity. Indeed, $\mathbf{4_{H\text{-}T}}$ has a good solubility in nonpolar solvents such as pentane or *n*-hexane. The $^{13}C\{^1H\}$ NMR spectroscopic data for $\mathbf{4_{H\text{-}H}}$ and $\mathbf{4_{H\text{-}T}}$ in C_6D_6 show for each isomer one set of mesitylimidazolide and two CO signals, consistent with either a C_s or C_2 molecular symmetry. Compared to the cod precursors ($\mathbf{3_{H\text{-}H}}$ and $\mathbf{3_{H\text{-}T}}$), the $^{13}C\{^1H\}$ NMR resonances of the imidazolide C2 are downfield shifted (δ 172.8 in $\mathbf{4_{H\text{-}H}}$ and δ 175.1 in $\mathbf{4_{H\text{-}T}}$). The IR spectra of $\mathbf{4_{H\text{-}H}}$ and $\mathbf{4_{H\text{-}T}}$ show three ν(CO) bands at 2060, 2037, 1954 and 2059, 2041, 1968 cm^{-1}, respectively, corresponding to the pattern for a dinuclear, folded tetracarbonyl framework.

Dalton Transactions Accepted Manuscript

View Article Online
DOI: 10.1039/C5DT02403J

Published on 23 July 2015. Downloaded by University of California - Santa Barbara on 28/07/2015 05:09:18.

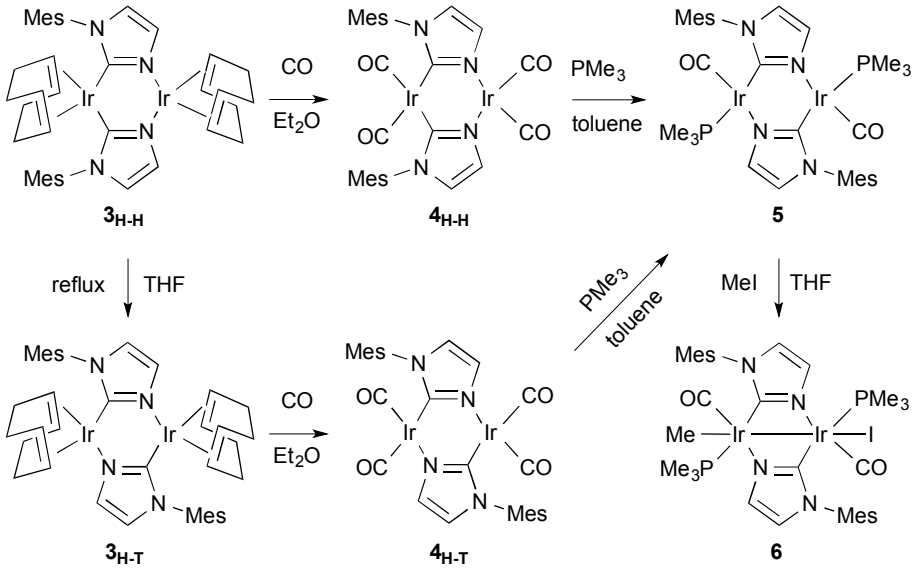

Scheme 7 Reactions of $\mathbf{3_{H\text{-}H}}$ and $\mathbf{3_{H\text{-}T}}$ with CO or PMe_3.

The reaction of $\mathbf{4_{H\text{-}H}}$ or $\mathbf{4_{H\text{-}T}}$ with 2.0 equiv. of trimethylphosphine in toluene at room temperature afforded the same red solid $[Ir(CO)(PMe_3)\{\mu\text{-}C_3H_2N_2(Mes)\text{-}\kappa C2,\kappa N3\}]_2$ (**5**), which shows two ν(CO) bands at 2000 and 1911 cm^{-1} in the infra-red spectrum (Scheme 7). According to the NMR spectra in C_6D_6, this complex contains one set of mesitylimidazolide, trimethylphosphine and CO signals. The imidazolide backbone protons at C4 and C5 are observed at δ 6.89 (d) and 6.68 (d, ^3J = 0.9 Hz) and the corresponding $^{13}C\{^1H\}$ NMR resonances at δ 128.3 and 120.1. In the $^{13}C\{^1H\}$ NMR spectrum, the resonances due to the CO and $C_{imidazolide}$ carbons are found at δ 181.4 (d, $J_{C\text{-}P}$ = 10.0 Hz) and 177.1 (d, $J_{C\text{-}P}$ = 112.0 Hz), respectively. The coordinated trimethylphosphine ligands give rise to a ^1H NMR resonance at δ 1.13 (d, $^2J_{H\text{-}P}$ = 8.7 Hz), a $^{13}C\{^1H\}$ NMR signal at δ 17.0 (d, $J_{C\text{-}P}$ = 31.6 Hz) and a singlet in $^{31}P\{^1H\}$ NMR at δ -24.1. All these data are consistent with a C_2 molecular symmetry for **5**, *i.e.* a H-T arrangement. The isomerization of the central core $Ir[\mu\text{-}C_3H_2N_2(Mes)\text{-}\kappa C2,\kappa N3]_2Ir$ from H-H to H-T on going from $\mathbf{4_{H\text{-}H}}$ to **5** has thus been triggered by phosphine substitution under mild conditions. The preference for the H-T arrangement is consistent with $\mathbf{3_{H\text{-}T}}$ being the thermodynamically favoured isomer of **3**.

Oxidative-Addition of MeI.

Treatment of **5** with a slight excess of MeI afforded the yellow complex $[Ir_2(CO)_2(PMe_3)_2(Me)I\{\mu\text{-}C_3H_2N_2(Mes)\text{-}\kappa C2,\kappa N3\}_2]$ (**6**) corresponding to a 1:1 addition product (Scheme 7). The observation in C_6D_6 of two sets of ^1H NMR signals for the mesitylimidazolide and trimethylphosphine protons and of $^{13}C\{^1H\}$ NMR signals for the CO ligands is consistent with a non-symmetric system. In the $^{13}C\{^1H\}$ NMR spectrum, the resonances of the $C_{imidazolide}$ carbons are significantly upfield shifted (δ 142.8 and 140.8 *vs.* δ 177.1 in **5**). The $^{31}P\{^1H\}$ NMR spectrum shows two close resonances at δ -46.6 and -48.9, consistent with similarly bonded but inequivalent phosphine ligands.[12a] Attempts to crystallize **6** were unsuccessful. The IR spectrum of **6** shows two ν(CO) bands at 2019 and 1952 cm^{-1}, indicative of weaker back-bonding from the metal to the CO ligands compared to **5** and consistent with the presence of iridium(II) centres in **6** where a formal metal-metal bond leads to a 18 electron count to each metal centre. In contrast to **5**, an NMR experiment showed that $\mathbf{3_{H\text{-}T}}$ reacted reversibly with MeI since placing a solution of the oxidative-addition product, obtained in the presence of excess MeI, under reduced pressure regenerated $\mathbf{3_{H\text{-}T}}$. Such a behaviour has been previously observed with diiridium pyrazolido-bridged complexes and explained by the steric hindrance caused by the cod ligands that prevents the iridium centres to get closer to each other in the oxidised product.[12h]

Synthesis and Characterisation of Diiridium Tetraethylene Complexes

Treatment of **1a** with 0.5 equiv. $[Ir(C_2H_4)_2(\mu\text{-}Cl)]_2$ at -78 °C in Et_2O led to the formation of the doubly C,N-bridged imidazolide dinuclear complex $[Ir(C_2H_4)_2\{\mu\text{-}C_3H_2N_2(Mes)\text{-}\kappa C2,\kappa N3\}]_2$ (**7**) as a blue solid in 77% yield (Scheme 8).

Dalton Transactions Accepted Manuscript

View Article Online
DOI: 10.1039/C5DT02403J

Published on 23 July 2015. Downloaded by University of California - Santa Barbara on 28/07/2015 05:09:18.

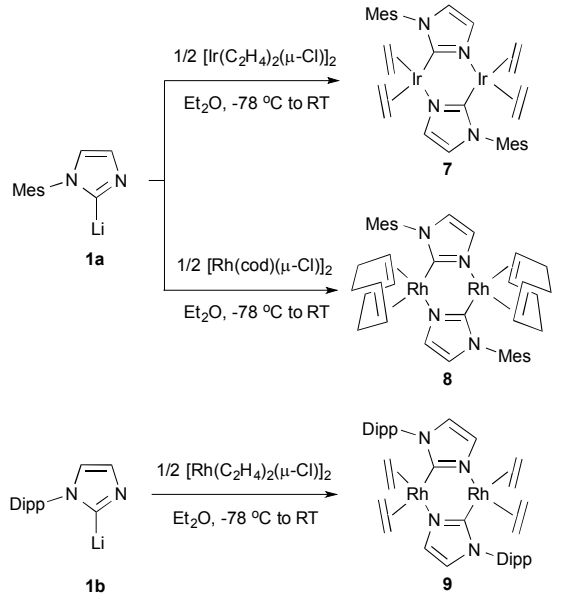

Scheme 8 Synthesis of the isolated dinuclear olefinic complexes **7**-**9**.

The colour of **7** is similar to that of other tetraethylene diiridium complexes reported in the literature.[13c] Its NMR spectra in C_6D_6 only showed one set of mesitylimidazolide signals. In the $^{13}C\{^1H\}$ NMR spectrum, the resonance of the $C_{imidazolide}$ is observed at δ 171.5. The imidazolide protons at C4 and C5 gave rise to an AX pattern at δ 7.09 (d) and 6.49 (d, ^3J = 1.5 Hz) and the corresponding $^{13}C\{^1H\}$ NMR resonances occurred at δ 124.6 and 122.0, respectively. In the ^1H NMR spectrum, two AA'BB' patterns are anticipated for the chemically-distinct coordinated ethylene ligands (trans to C and trans to N).[13c,18] The resolution of the spectra did not allow to extract all the corresponding coupling constants. Nevertheless, one AA'BB' pattern with δ_B 3.13 and δ_A 2.89 and a second AA'BB' pattern with δ_B 2.63 and δ_A 2.36 were observed (Fig. S2).[19] Since the ^1H NMR chemical shifts of the mesityl and imidazolide groups are similar to those of $\mathbf{3_{H\text{-}T}}$, the arrangement of **7** should also be H-T but attempts to crystallize **7** were unsuccessful.

Synthesis and Characterisation of Dirhodium cod and Tetraethylene Complexes

To extend the scope of the reactivity of **1a**, it was treated with 0.5 equiv. of $[Rh(cod)(\mu\text{-}Cl)]_2$, and the new complex $[Rh(cod)\{\mu\text{-}C_3H_2N_2(Mes)\text{-}\kappa C2,\kappa N3\}]_2$ (**8**) was isolated (Scheme 8). As for **8**, the $^{13}C\{^1H\}$ NMR spectrum of **8** in C_6D_6 only showed one set of mesitylimidazolyl signals and a doublet due to C2 at δ 176.2 ($J_{C\text{-}Rh}$ = 50.4 Hz). The protons at C4 and C5 were observed in the ^1H NMR spectrum at δ 6.96 and 6.51 as two broad singlets (the $^3J_{H\text{-}H}$ coupling was not resolved) and the corresponding $^{13}C\{^1H\}$ resonances were found at δ 126.8 and 120.3. The UV-visible-NIR absorption spectrum of **8** in CH_2Cl_2 is shown in Fig. S3. Orange single crystals of **8** suitable for X-ray diffraction were grown from a toluene solution at 0 °C under argon. The molecular structure of **8** is shown in Fig. 3, with selected bond lengths and angles. This complex adopts a H-T arrangement and the same boat conformation as its iridium analog. The separation between the two Rh atoms is 3.2117(4) Å, which is too long to represent a direct metal-metal interaction. Each rhodium atom is in a 16 valence electron configuration and adopts an approximate square planar geometry, defined by two olefinic bonds of the 1,5-cyclooctadiene ligand, one carbon atom of one imidazolide and one nitrogen atom of the another bridging imidazolide ligand.

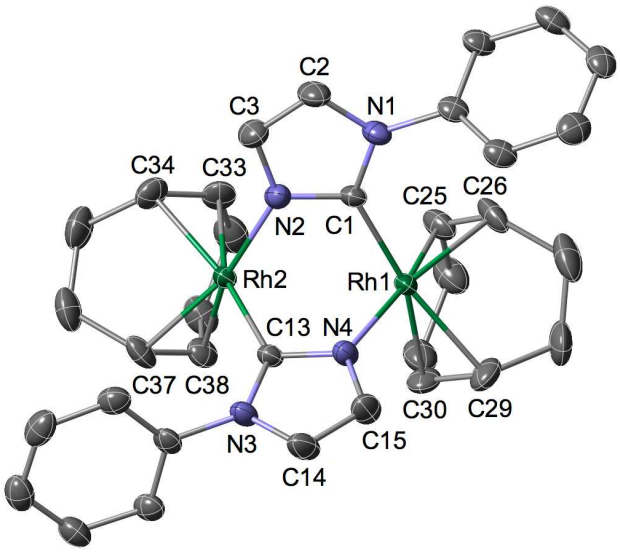

Fig 3 View of the molecular structure of **8**, H atoms and methyl groups are omitted for clarity. Thermal ellipsoids are at the 30% level. Selected bond lengths (Å) and angles (°): Rh1···Rh2 3.2117(4), C1–N1 1.376(3), C1–N2 1.342(3), Rh1–C1 2.045(2), Rh1–N4 2.079(2), Rh1–C25 2.135(3), Rh1–C26 2.117(3), Rh1–C29 2.188(3), Rh1–C30 2.171(3), C25–C26 1.382(4), C29–C30 1.372(4), C13–N3 1.378(3), C13–N4 1.345(3), Rh2–N2 2.067(3), Rh2–C13 2.043(4), Rh2–C33 2.172(3), Rh2–C34 2.183(3), Rh2–C37 2.118(3), Rh2–C38 2.122(3), C33–C34 1.376(4), C37–C38 1.392(4); N1–C1–N2 106.7(2), N3–C13–N4 106.3(2), C1–Rh1–N4 85.73(9), C25–Rh1–C26 37.9(1), C26–Rh1–C29 82.3(1), C29–Rh1–C30 36.7(1), C30–Rh1–C25 81.4(1), N2–Rh2–C13 86.27(9), C33–Rh2–C34 36.8(1), C34–Rh2–C37 82.1(1), C37–Rh2–C38 38.3(1), C38–Rh2–C33 81.5(1).

The reaction of **1b** with $[Rh(C_2H_4)_2(\mu\text{-}Cl)]_2$ at -78 °C in Et_2O afforded $[Rh(C_2H_4)_2\{\mu\text{-}C_3H_2N_2(Dipp)\text{-}\kappa C2,\kappa N3\}]_2$ (**9**) (Scheme 8). Its NMR spectrum in C_6D_6 only showed one set of Dipp imidazolide signals and a doublet due to C2 at δ 175.1 ($J_{C\text{-}Rh}$ = 49.0 Hz). The resonances of the H atoms at the backbone carbons C4 and C5 were observed at δ 7.02 and 6.64, respectively, as two singlets, and the corresponding $^{13}C\{^1H\}$ NMR resonances at δ 125.9 and 122.8. In the ^1H NMR spectrum, like in **7**, two AA'BB' patterns are anticipated for the chemically distinct coordinated ethylene ligands.[13c,18] However, the resolution of the spectra did not allow extraction of all the corresponding coupling constants. Nevertheless one AA'BB' pattern with δ_B 3.65 and δ_A 3.58 and a second AA'BB' pattern with δ_B 2.86 and δ_A 2.62 were observed (Fig. S4).[19] Purple single

Dalton Transactions Accepted Manuscript

View Article Online
DOI: 10.1039/C5DT02403J

Published on 23 July 2015. Downloaded by University of California - Santa Barbara on 28/07/2015 05:09:18.

crystals of **9** suitable for X-ray diffraction were grown from *n*-hexane solution at -30 °C under ethylene atmosphere. A similar reaction using **1a** instead of **1b** proceeded similarly (^{1}H monitoring) although a well-characterised solid product could not be obtained due to limited solubility in hexane from which **9** could be crystallised. The molecular structure of **9** is shown in Fig. 4, with selected bond lengths and angles. The structure of **9** adopts a boat conformation and like in **8**, the arrangement of the bridging ligands is of the H-T type. The separation between two Rh atoms is 3.3146(9) Å, which is again too long to represent a direct bonding interaction. Each 16 electron rhodium atom adopts an approximately square planar geometry, defined by two ethylene ligands, one carbon atom of one imidazolido and one nitrogen atom of the other bridging imidizolido ligand. Like in $\mathbf{3_{H\text{-}T}}$, the metrical data indicate a more pronounced double bond character for the N-C bond located in the bridging part of the ligands.

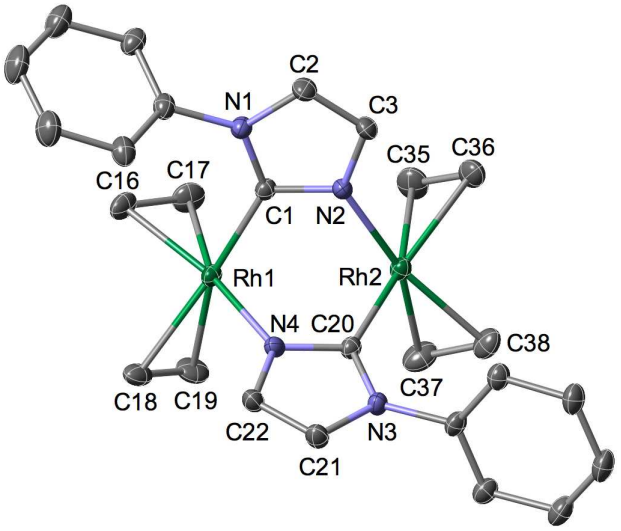

Fig. 4 View of the molecular structure of **9**, H atoms and isopropyl groups are omitted for clarity. Thermal ellipsoids are at the 30% level. Selected bond lengths (Å) and angles (°): Rh1···Rh2 3.3146(9), C1–N1 1.372(3), C1–N2 1.344(3), Rh1–C1 2.040(3), Rh1–N4 2.081(2), Rh1–C16 2.141(3), Rh1–C17 2.125(3), Rh1–C18 2.208(3), Rh1–C19 2.192(3), C16–C17 1.369(5), C18–C19 1.351(5), C20–N3 1.379(3), C20–N4 1.342(3), Rh2–N2 2.080(2), Rh2–C20 2.041(3), Rh2–C35 2.202(3), Rh2–C36 2.211(3), Rh2–C37 2.129(3), Rh2–C38 2.124(3), C35–C36 1.354(5), C37–C38 1.385(5); N1–C1–N2 106.7(2), N3–C20–N4 106.4(2), C1–Rh1–N4 84.6(1), C16–Rh1–C17 37.4(1), C17–Rh1–C19 89.2(2), C18–Rh1–C19 35.8(1), C16–Rh1–C18 86.9(1), N2–Rh2–C20 84.9(1), C35–Rh2–C36 35.7(1), C36–Rh2–C38 87.0(1), C37–Rh2–C38 38.0(1), C35–Rh2–C37 89.1(2).

Electrochemical investigations.

Since a two-electron oxidation of the dinuclear unit could formally give an Ir(II)-Ir(II) complex or a mixed-valence Ir(I)/Ir(III) complex in which only one metal centre would have been formally oxidised, we became interested in studying the redox behaviour of representatives of these dinuclear complexes, in particular, with respect to the two possible H-T or H-H arrangements of the bridging ligands, since they lead to a symmetrical or unsymmetrical electronic environment of the metal centres, respectively. An electrochemical investigation of complexes $\mathbf{3_{H\text{-}T}}$ and **8** was carried out by cyclic voltammetry and rotating disk voltammetry in CH_2Cl_2 + 0.1 M [*n*-Bu_4N]PF_6. Cyclic voltammograms of $\mathbf{3_{H\text{-}T}}$ and **8** with added ferrocene are presented in Figs. S5 and S6 (see ESI) and show reversible processes. In contrast, irreversible oxidation was observed by cyclic voltammetry in the case of complex $\mathbf{3_{H\text{-}H}}$ (see Fig. S7 in ESI)

As shown in Fig. 5 and Table 1, two successive oxidations have been detected in the case of $\mathbf{3_{H\text{-}T}}$. The first oxidation step occurs at -0.45 V *vs.* Fc^+/Fc and corresponds to a reversible electron transfer, while the second step presents an irreversible oxidation peak at +0.67 V *vs.* Fc^+/Fc.

The number of electrons exchanged during the first oxidation step was determined by exhaustive coulometry. During the electrolysis, the oxidation current decreased exponentially with time. When this current reached the residual value measured in the absence of electroactive material, typically after 4 h under the above conditions, the number of electrons transferred was 0.9/molecule of $\mathbf{3_{H\text{-}T}}$, which strongly suggests that oxidation of only one Ir(I) centre to Ir(II) has occurred, leading to the mixed-valent Ir(I)/Ir(II) intermediate. Attempts to chemically oxidize $\mathbf{3_{H\text{-}T}}$ using AgOTf in CH_2Cl_2 gave intractable mixture of species.

Table 1. Electrochemical data for $\mathbf{3_{H\text{-}T}}$, $\mathbf{3_{H\text{-}H}}$ and **8**.[a]

Complex		
$\mathbf{3_{H\text{-}T}}$	-0.45 (64)	+0.67[b]
$\mathbf{3_{H\text{-}H}}$	-1.23[b]	-0.39[b]
8	-0.40 (63)	+0.58[b]

[a] All potentials in V *vs.* Fc^+/Fc were obtained from cyclic voltammetry in CH_2Cl_2 containing 0.1 mol L^{-1} [*n*-Bu_4N]PF_6. Scan rate = 0.1 V s^{-1}. Working electrode: glassy carbon electrode. The given half-wave potentials in the case of the reversible couple are equal to $E_{1/2} = (E_{pa}\text{-}E_{pc})/2$. In bracket: ($\Delta E_p$, peak splitting in mV at a scan rate of 0.1 Vs^{-1}). [b] Irreversible electron transfer.

Dalton Transactions Accepted Manuscript

View Article Online
DOI: 10.1039/C5DT02403J

Published on 23 July 2015. Downloaded by University of California - Santa Barbara on 28/07/2015 05:09:18.

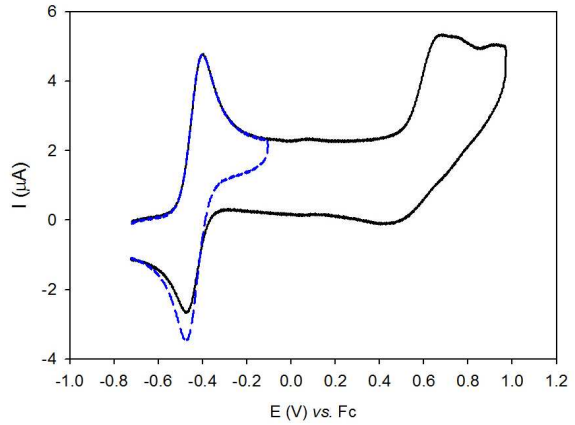

Fig. 5 Cyclic voltammograms of $\mathbf{3}_{\mathbf{H\text{-}T}}$ (CH_2Cl_2 + 0.1 M [*n*-Bu_4N]PF_6, glassy carbon electrode, scan rate 0.1 Vs^{-1}, *vs.* Fc^+/Fc).

In-situ spectroelectrochemical studies have been carried out, under argon atmosphere, to gain further insight into the nature of the electrogenerated species during this first reversible oxidation (Fig. 6).

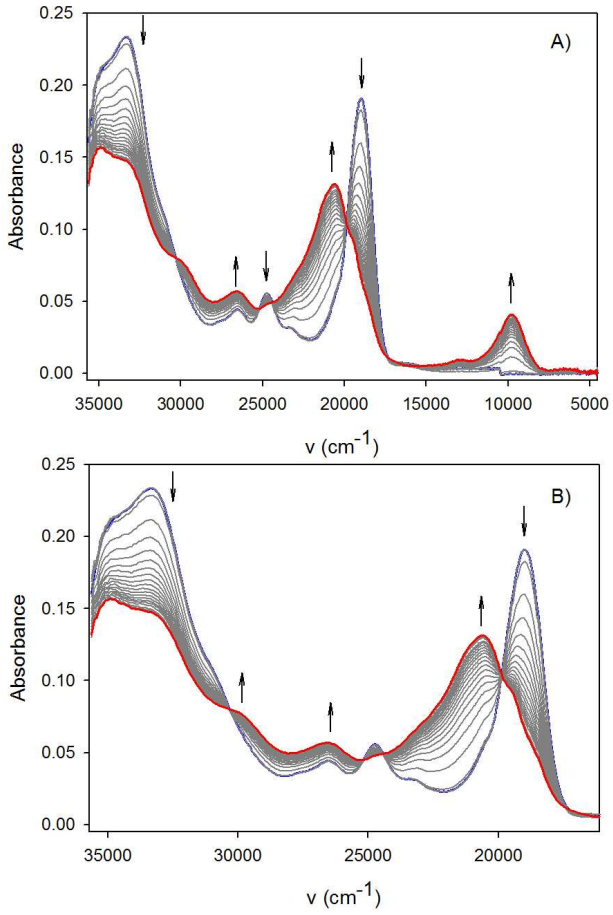

Fig. 6 A) Time-resolved UV-visible-NIR spectra of $\mathbf{3}_{\mathbf{H\text{-}T}}$ for the first oxidation step (transition Ir(I)/Ir(I) to Ir(I)/Ir(II)) in CH_2Cl_2 + 0.1 M [*n*-Bu_4N]PF_6 (spectra recorded every 5 s). B) UV-visible spectral evolution for the first oxidation step.

For $\mathbf{3}_{\mathbf{H\text{-}T}}$, time resolved UV-Vis-NIR spectroelectrochemistry data were recorded during cyclic voltammetry between -0.70 V and +0.20 V *vs.* Fc^+/Fc (scan rate 20 mVs^{-1}). As seen from the array of spectra depicted in Fig. 6 (and Fig. S8 for the plot *versus* λ (nm)), during the oxidation the generated Ir(I)/Ir(II) species is characterised by low-energy intervalence charge transfer (IVCT) bands in the near infrared region at 1024 nm. On the reverse potential scan, a decrease of the intensity for this IVCT band was observed and the oxidized Ir(I)/Ir(II) system reverted quantitatively to the initial Ir(I)/Ir(I) species.

From the results obtained by cyclic voltammetry (reversible oxidation at -0.45 V *vs.* Fc^+/Fc), exhaustive coulometry (one-electron process) and spectroelectrochemistry (new NIR band at λ_{max} = 1024 nm for the oxidized system), it can be concluded that $\mathbf{3}_{\mathbf{H\text{-}T}}$ undergoes a one electron oxidation on the metal generating the mixed-valent Ir(I)/Ir(II) system, in equilibrium with Ir(II)/Ir(I), and giving rise to an IVCT band in the NIR region.

For comparison, we examined a H-T dirhodium complex. Features similar to those for $\mathbf{3}_{\mathbf{H\text{-}T}}$ were observed with **8** and the mixed-valent system Rh(I)/Rh(II). The cyclic voltammogram shows two successive oxidations, the first at -0.40 V *vs.* Fc^+/Fc corresponds to a reversible electron transfer, while the second step is associated to an irreversible oxidation process at +0.58 V *vs.* Fc^+/Fc (Fig. 7). Again, exhaustive coulometry indicated a number of electrons transferred of 0.9/molecule for **8**, leading to the mixed-valent intermediate Rh(I)/Rh(II).

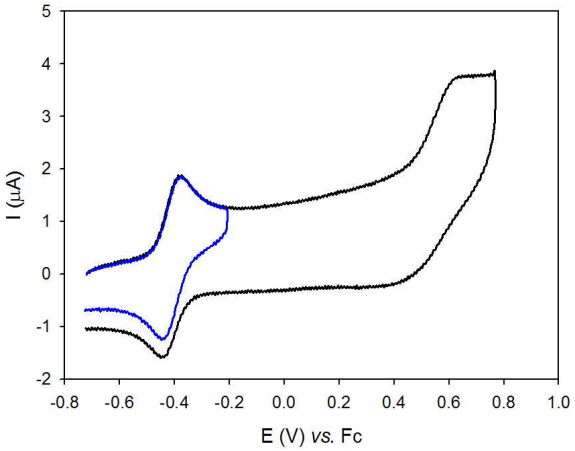

Fig. 7 Cyclic voltammograms of **8** (CH_2Cl_2 + 0.1 M [*n*-Bu_4N]PF_6, Glassy carbon electrode, scan rate 0.1 Vs^{-1}, *vs.* Fc^+/Fc).

Spectroelectrochemistry measurements at the first oxidation process evidenced a new low-energy intervalence charge transfer (IVCT) band around 1073 nm, which is in good agreement with the formation of a mixed-valent intermediate Rh(I)/Rh(II) (Fig. 8 and Fig. S9 for the plot *versus* λ (nm)). The new band at 612 nm might correspond to the Rh(II).

For **8** and for $\mathbf{3}_{\mathbf{H\text{-}T}}$, we observed one additional band at 612 nm and 781 nm, respectively. In studies on mixed-valent Ir(I)/Ir(II) or Rh(I)/Rh(II) intermediates, similar bands were also

Dalton Transactions Accepted Manuscript

View Article Online
DOI: 10.1039/C5DT02403J

Published on 23 July 2015. Downloaded by University of California - Santa Barbara on 28/07/2015 05:09:18.

observed, but not at the same wavelength, because of the presence of different ligands.[20] Such bands may be attributed to the Ir(II) or Rh(II) component of the complexes.

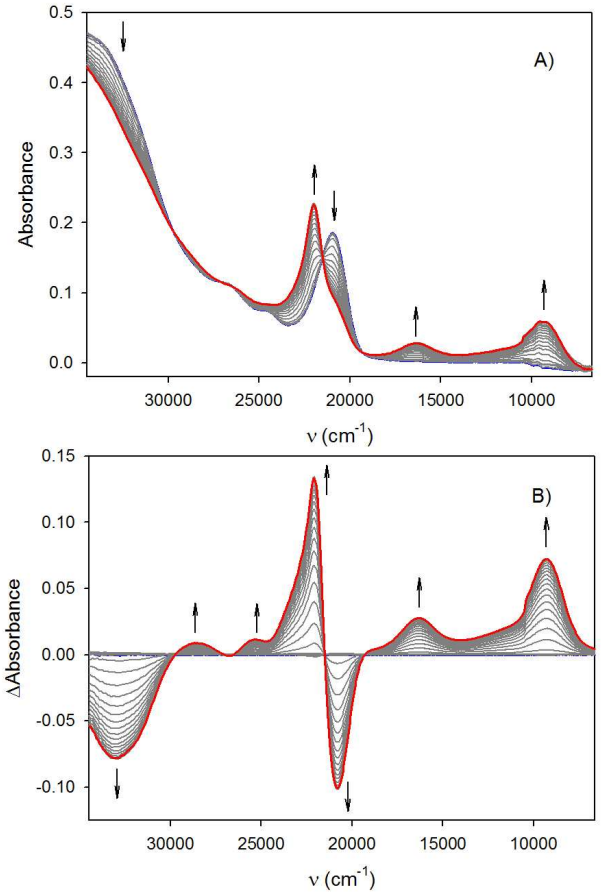

Fig. 8 A) Time-resolved UV-visible-NIR spectra of **8** for the first oxidation step (transition Rh(I)/Rh(I) to Rh(I)/Rh(II)) in CH_2Cl_2 + 0.1 M [*n*-Bu_4N]PF_6 (spectra recorded every 5 s). B) Time-resolved UV-visible-NIR differential spectra for the first oxidation step.

For a dinuclear system, the electronic coupling calculated from the Hush equation[21] decreases with the distance between the metal centres. Hush proposed that the electronic coupling could be extracted from the intervalence band shape according to eq (1):

$$H_{ab} = 0.0206(\varepsilon_{max}\Delta\nu_{1/2}\lambda)^{1/2}/d_{ab} \quad (1)$$

where ε_{max} ($M^{-1}\cdot cm^{-1}$) is the maximum intensity, $\Delta\nu_{1/2}$ (cm^{-1}) is the width at half-height, λ (cm^{-1}) is the energy maximum band (E_{op}), and d_{ab} (Å) is the diabatic electron-transfer distance. E_{op} occurs at 9823 cm^{-1} (λ_{max} = 1018 nm) and at 9320 cm^{-1} (λ_{max} = 1073 nm) for $\mathbf{3_{H\text{-}T}}$ and **8**. The measured $\Delta\nu_{1/2}$ values for $\mathbf{3_{H\text{-}T}}$ and **8** are 47393 cm^{-1} and 40486 cm^{-1}, respectively. According to eq (1), the corresponding calculated electronic couplings are $H_{Ir\text{-}Ir}$ = 3960 cm^{-1} and $H_{Rh\text{-}Rh}$ = 4746 cm^{-1}. Thus, the energy of the intervalence band for **8** is shifted toward lower energies in comparison with $\mathbf{3_{H\text{-}T}}$, reflecting the decrease of the energy with the intermetallic distance ($d_{Ir\text{-}Ir}$ = 3.141 Å, $d_{Rh\text{-}Rh}$ = 3.212 Å).

The transition from charge localized to charge-delocalized (which are also called class II and class III, respectively, in the Robin–Day terminology)[22] occurs at $\lambda = 2H_{ab}$, so mixed-valent (MV) compounds with $\lambda > 2H_{ab}$ are charge-localized and those with $\lambda \sim 2H_{ab}$ are charge-delocalized. In our case:

$\mathbf{3_{H\text{-}T}}$: λ (9823 cm^{-1}) > $2H_{ab}$ (2 x 3960 = 7920 cm^{-1})

8: λ (9320 cm^{-1}) is ~ $2H_{ab}$ (2 x 4746 = 9492 cm^{-1})

For **8**, λ (9320 cm^{-1}) is ~ $2H_{ab}$

These data thus suggest that $\mathbf{3_{H\text{-}T}}$ is a charge-localized while **8** is a charge-delocalized system under the conditions of our room temperature measurements.

EPR measurements.

EPR spectroscopy constitutes a highly suitable tool to evaluate the electronic structure of metal complexes with unpaired electrons, especially on heavy metal centres. At low temperature, the average <*g*> value and the anisotropy (Δg) calculated from the principal values of the *g*-tensor afford a qualitative estimate of the extent of electron localization over the metal and/or over the ligand.[23] We thus wanted to examine in more detail the electronic structure of the mixed-valent Ir(I)/Ir(II) and Rh(I)/Rh(II) species. The oxidized species were generated at room temperature by electrolysis after consumption of about 0.9 electron/molecule and the resulting solutions were transferred into an EPR tube under argon. The X-band EPR spectrum in frozen CH_2Cl_2 solution of Ir(I)/Ir(II) (the oxidized species of $\mathbf{3_{H\text{-}T}}$) exhibited a signal with an axial symmetry (Fig. 9) with $g_1 = g_2 = 1.987$ and $g_3 = 2.123$ values (see Table 2). Increasing the temperature to ambient caused the EPR signal to disappear. In the case of the Rh(I)/Rh(II) system obtained by oxidation of **8**, the EPR spectrum at low temperature displayed a rhombic signal (Fig. S10 in ESI). At room temperature, a very weak EPR signal is recorded with only one line centred at around g = 2.00 without hyperfine structure. Satisfying simulations were obtained with one or two equivalent ^{103}Rh nucleus (I = 1/2 isotopic abundance 100%) and in order to discriminate between the two possibilities DFT calculations were performed. The structure of the Rh(I)/Rh(II) complex was subjected to geometry optimization (Fig. S11) and its electronic structure was investigated (Fig. S12). Mulliken population analysis indicates an equally distributed spin density between the two rhodium atoms with positive spin populations found at Rh(1) (0.49) and Rh(2) (0.49). The spin density of the Rh atoms accounts for 90% of the total spin density and the remaining 10% are spread over the ligands. The Singly Occupied Molecular Orbital (SOMO) of the complex displays 90% Rh character and features the σ antibonding interaction between the Rh $3d_z^2$ orbitals. The EPR parameters arising from the spectral simulation for two equivalent ^{103}Rh nuclei are reported in Table 2. The results of the DFT calculations for the Ir(I)/Ir(II) system are similar to those obtained for Rh(I)/Rh(II) and also suggest a delocalized mixed-valent species (Figs. S13 and S14).

Dalton Transactions Accepted Manuscript

View Article Online
DOI: 10.1039/C5DT02403J

Published on 23 July 2015. Downloaded by University of California - Santa Barbara on 28/07/2015 05:09:18.

Table 2. EPR parameters of the oxidized complexes

	g_1	g_2	g_3	<g>[a]	Δg[b]	?G	?G	?G
Ir(I)/Ir(II)	1.987	1.987	2.123	2.033	0.136	-	-	-
Rh(I)/Rh(II)	1.993	2.031	2.105	2.043	0.112	33	18	27

[a] $\langle g\rangle = [(g_1^2 + g_2^2 + g_3^2)/3]^{1/2}$; [b] $\Delta g = g_3 - g_1$

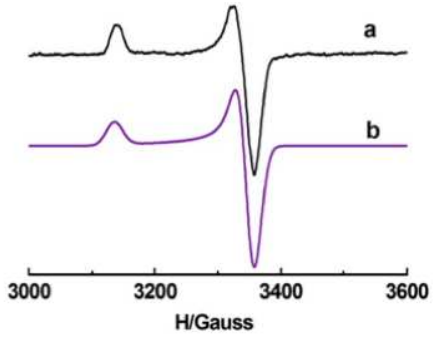

Fig. 9 EPR spectra of the Ir(I)/Ir(II) system electrochemically generated from $\mathbf{3_{H\text{-}T}}$ system electrochemically generated in CH_2Cl_2 at 100 K: a) Experimental spectrum b) Simulated spectrum.

The oxidized forms are characterised by a *g* anisotropy and the average *g* values are significantly larger than for the free electron (2.0023). Such features may imply that the Ir and Rh centres contribute substantially to the experimental magnetic anisotropy and thus to SOMO.

Attempted catalytic transfer dehydrogenation of cyclooctane using iridium complexes $\mathbf{3_{H\text{-}T}}$, $\mathbf{4_{H\text{-}T}}$, 5 and 7 as precatalysts.

Iridium pincer complexes have shown very promising catalytic properties in alkane dehydrogenation reactions,[24] due to their high thermal stability and high efficiency. The synergistic action of two reactive sites in close proximity could be seen as a key element in the design of powerful catalysts. This prompted us to explore the catalytic activity of these dinuclear iridium complexes towards alkane dehydrogenation. The reaction of cyclooctane (COA) and *t*-butylethylene (TBE), as sacrificial olefin, to form cyclooctene (COE) and *t*-butylethane (TBA) catalyzed by the POCOP iridium pincer complex[25] was employed in the benchmark reaction.

Table 3. Catalytic transfer dehydrogenation of cyclooctane in the presence of *t*-butylethylene with $\mathbf{3_{H\text{-}T}}$, $\mathbf{4_{H\text{-}T}}$, **5** and **7**[a]

entry	catalyst	TON[b]	TOF[c]/h^{-1}
1	$\mathbf{3_{H\text{-}T}}$	4.6	0.46
2	$\mathbf{4_{H\text{-}T}}$	-	-
3	**5**	5.8	0.58
4	**7**	62.4	6.24

[a] Reaction conditions: [Ir_2] catalyst (0.010 mmol), COA (4.0 mL, 30.3 mmol), TBE (0.40 mL, 3.1 mmol), 200 °C, 10 h; [b] the number of moles of COA that a mole of [Ir_2] catalyst can convert in 10 h; [c] turnover number per hour.

The results of preliminary experiments on the catalytic transfer dehydrogenation of COA to COE are summarized in Table 3. Using complex **7** as precursor gave better results and 2.06% of the cyclooctane was converted to *cis*-cyclooctene at a TOF of 6.24 h^{-1}. This higher value compared to the other pre-catalysts is probably due to the easier de-coordination of the ethylene ligands from the iridium centres, which facilitates the metal-alkane interactions.

Conclusions

In this work, we have provided a more detailed investigation on dinuclear Ir(I) and Rh(I) complexes containing a bridging 1-arylimidazolide ligand, C2 and N3-bound to the metals.[16b] Initial deprotonation of 1-arylimidazoles (aryl = mesityl (Mes), 2,6-diisopropylphenyl (Dipp)) by *n*-butyl lithium in pentane at -30 °C was carried out to afford the corresponding derivatives (1-aryl-1*H*-imidazol-2-yl)lithium (**1a,b**) which were then used to prepare the doubly C,N-bridged dinuclear Ir(I) complexes **3**. These Ir(I) complexes exist in two isomeric forms, $\mathbf{3_{H\text{-}H}}$ which is the head-to-head isomer of C_S symmetry, and $\mathbf{3_{H\text{-}T}}$, the head-to-tail isomer of C_2 symmetry, which is thermodynamically more stable. The X-ray diffraction data suggest electron delocalisation within the N···C···N system and thus some carbene character for the Ir-bound imidazolide carbon atom, that is more pronounced in $\mathbf{3_{H\text{-}H}}$. The metal-bound imidazolide may be viewed as a deprotonated pNHC system. When the tetracarbonyl derivatives $\mathbf{4_{H\text{-}H}}$ and $\mathbf{4_{H\text{-}T}}$ were reacted with PMe_3, one CO ligand was displaced from each Ir centre and only one isomer was formed, **5**, in which the imidazolide ligands are

Dalton Transactions Accepted Manuscript

View Article Online
DOI: 10.1039/C5DT02403J

Published on 23 July 2015. Downloaded by University of California - Santa Barbara on 28/07/2015 05:09:18.

bound in a H-T manner This ligand arrangement was retained in the formally metal-metal bonded, d^7-d^7 Ir(II)-Ir(II) complex, **6**, resulting from oxidative-addition of MeI across **5**. From the results obtained by cyclic voltammetry, exhaustive coulometry and spectroelectrochemistry, it was concluded that $\mathbf{3_{H\text{-}T}}$ undergoes a metal-based one electron oxidation to generate the mixed-valent Ir(I)/Ir(II) system, in equilibrium with Ir(II)/Ir(I), characterised by an IVCT band in the NIR region.

EPR studies combined with DFT calculations suggested that the Ir and Rh centres contribute substantially to the experimental magnetic anisotropy in the oxidized species and thus to the SOMO. These data evidenced that both Ir(II)/Ir(I) and Rh(II)/Rh(I) complexes are delocalized mixed-valent species.

The dinuclear iridium complexes were found to be only moderately active pre-catalysts in the reaction of cyclooctane and *t*-butylethylene to form cyclooctene and *t*-butylethane. Whether these results are directly linked to a difficulty to access coordinatively unsaturated and reactive species or to an inhibiting effect of the cod ligands cannot be stated at this stage. In favour of the latter hypothesis is that slightly better performances were obtained with the tetraethylene complex **7**, may be due to the favourable lability of the ethylene ligands.

Experimental

General Considerations

All manipulations involving organometallics were performed under argon in a Braun glove-box or using standard Schlenk techniques. Solvents were dried using standard methods and distilled over sodium/ benzophenone under argon prior use or passed through columns of activated alumina and subsequently purged with argon. The starting materials $[Rh(cod)(\mu\text{-}Cl)]_2$,[26] $[Ir(C_2H_4)_2(\mu\text{-}Cl)]_2$[12h] and $[Rh(C_2H_4)_2(\mu\text{-}Cl)]_2$[27] were prepared according to the literature and $[Ir(cod)(\mu\text{-}Cl)]_2$ is commercially available from Johnson Matthey PLC. NMR spectra of complexes were recorded on a Bruker 300 MHz, 400 MHz, 500 MHz or 600 MHz instrument at ambient temperature and referenced using the proton (^{1}H) or carbon (^{13}C) resonance of the residual solvent, with downfield shifts reported as positive. Assignments are based on ^{1}H, ^{1}H-COSY, ^{1}H-NOESY, ^{1}H/^{13}C-HSQC, and ^{1}H/^{13}C-HMBC experiments. ^{31}P{^{1}H} NMR spectra were recorded on a Bruker Avance 300 instrument at 121.49 MHz using H_3PO_4 (85% in D_2O) as external standard. IR spectra were recorded in the region 4000–100 cm^{-1} on a Nicolet 6700 FT-IR spectrometer (ATR mode, diamond crystal). Elemental analyses were performed by the "Service de microanalyses", Université de Strasbourg.

Synthetic procedures

(1-Mesityl-1*H*-imidazol-2-yl)lithium (1a). To a stirred solution of 1-mesitylimidazole (1.49 g, 8.0 mmol) in pentane (30 mL) was added dropwise a solution of *n*-BuLi (1.6 M in *n*-hexane, 5.0 mL, 8.0 mmol) at -78 °C over 2 min. The reaction mixture was stirred for 1 h at -30 °C, then allowed to warm to room temperature and stirred for another 2 h. The resulting clear orange solution was evaporated in vacuo. The residue was washed with pentane (3 × 5 mL) to yield a white powder which was collected by filtration and dried in vacuo (1.08 g, 70%). ^{1}H NMR (500 MHz, THF-d_8): δ 7.04 (s, 1H, NC*H*CHN$_{(mesityl)}$), 6.83 (s, 2H, aryl-*H*), 6.70 (s, 1H, NCHC*H*N$_{(mesityl)}$), 2.25 (s, 3H, *p*-C*H*$_{3(mesityl)}$), 1.95 (s, 6H, *o*-C*H*$_{3(mesityl)}$). ^{13}C{^{1}H} NMR (125 MHz, THF-d_8): δ 205.8 (N*C*N$_{(mesityl)}$), 142.3 (*C*$_{(mesityl)}$), 136.5 (*C*$_{(mesityl)}$), 135.5 (*C*$_{(mesityl)}$) 128.3 (*C*H$_{(mesityl)}$), 127.9 (N*C*HCHN$_{(mesityl)}$), 116.8 (NCH*C*HN$_{(mesityl)}$), 20.9 (*p*-*C*H$_{3(mesityl)}$), 18.2 (*o*-*C*H$_{3(mesityl)}$).

(1-(2,6-Diisopropylphenyl)-1*H*-imidazol-2-yl)lithium (1b). To a stirred solution of 1-(2,6-diisopropylphenyl)-imidazole (1.83 g, 8.0 mmol) in pentane (30 mL) was added dropwise a solution of *n*-BuLi (1.6 M in *n*-hexane, 5.0 mL, 8.0 mmol) at -78 °C over 2 min. Then the reaction mixture was allowed to warm to room temperature and stirred for another 2 h. The precipitate was collected by filtration, washed with pentane and dried in vacuo to obtain a white powder (1.72 g, 92%). ^{1}H NMR (500 MHz, THF-d_8): δ 7.19 (t, ^3J = 7.6 Hz, 1H, *p*-aryl-*H*), 7.11 (d, ^3J = 7.6 Hz, 2H, *m*-aryl-*H*), 7.04 (s, 1H, NC*H*CHN$_{(Dipp)}$), 6.81 (s, 1H, NCHC*H*N$_{(Dipp)}$), 2.72 (sept, ^3J = 6.9 Hz, 2H, C*H*(CH$_3$)$_2$), 1.04 (d, ^3J = 6.9 Hz, 6H, CH(C*H*$_3$)$_2$), 1.03 (d, ^3J = 6.9 Hz, 6H, CH(C*H*$_3$)$_2$). ^{13}C{^{1}H} NMR (125 MHz, THF-d_8): δ 202.3 (N*C*N$_{(Dipp)}$), 147.4 (*C*$_{(Dipp)}$), 142.2 (*C*$_{(Dipp)}$), 127.4 (N*C*HCHN$_{(Dipp)}$), 127.1 (*C*H$_{(Dipp)}$), 123.0 (*C*H$_{(Dipp)}$), 119.0 (NCH*C*HN$_{(Dipp)}$), 28.3 (*C*H(CH$_3$)$_2$), 25.1 (CH(*C*H$_3$)$_2$), 24.3 (CH(*C*H$_3$)$_2$).

1-Mesitylimidazolyl(cycloocta-1,5-diene)iridium(I) chloride [Ir(cod)Cl{$C_3H_3N_2$(Mes)-κN3}] (2). A solution of 1-mesitylimidazole (0.028 g, 0.15 mmol) in THF (2 mL) was added to a stirred solution of $[Ir(cod)(\mu\text{-}Cl)]_2$ (0.050 g, 0.074 mmol) in THF (2 mL). The mixture was stirred for 1 h at room temperature and then the volatiles were removed in vacuo. The residue was washed with pentane (3 × 2 mL) and dried under vacuum to give a yellow powder (0.074 g, 0.14 mmol, 94%). ^{1}H NMR (500 MHz, CD_2Cl_2): δ 8.27 (apparent t, ^4J = 1.4 Hz, 1H, NC*H*N), 7.28 (apparent t, $^{3,4}J$ = 1.4 Hz, 1H, NC*H*CHN$_{(mesityl)}$), 6.99 (s, 2H, aryl-*H*), 6.96 (apparent t, $^{3,4}J$ = 1.4 Hz, 1H, NCHC*H*N$_{(mesityl)}$), 4.20 (br s, 2H, C*H*$_{(cod)}$), 3.71 (br s, 2H, C*H*$_{(cod)}$), 2.33 (s, 3H, *p*-C*H*$_{3(mesityl)}$), 2.27 (m, 4H, C*H*$_{2(cod)}$), 1.98 (s, 6H, *o*-C*H*$_{3(mesityl)}$), 1.62 (m, 2H, C*H*$_{2(cod)}$), 1.51 (m, 2H, C*H*$_{2(cod)}$). ^{13}C{^{1}H} NMR (125 MHz, CD_2Cl_2): δ 140.4 (N*C*HN), 140.3 (*p*-*C*$_{(mesityl)}$), 135.3 (*o*-*C*$_{(mesityl)}$), 132.6 (*ipso*-*C*$_{(mesityl)}$), 129.5 (*m*-*C*$_{(mesityl)}$), 126.9 (N*C*HCHN$_{(mesityl)}$), 121.5 (NCH*C*HN$_{(mesityl)}$), 67.1 (*C*H$_{(cod)}$), 58.2 (*C*H$_{(cod)}$), 32.3 (*C*H$_{2(cod)}$), 31.5 (*C*H$_{2(cod)}$), 21.2 (*p*-*C*H$_{3(mesityl)}$), 17.5 (*o*-*C*H$_{3(mesityl)}$). Anal. Calcd for $C_{20}H_{26}ClIrN_2$ (%): C, 46.01; H, 5.02; N, 5.37. Found: C, 45.79; H, 5.11; N, 5.90.

[Ir(cod){μ-$C_3H_2N_2$(Mes)-κC2,κN3}]$_2$ ($\mathbf{3_{H\text{-}H}}$). To a stirred solution of **1a** (0.100 g, 0.52 mmol) in Et_2O (10 mL) was added a solution of $[Ir(cod)(\mu\text{-}Cl)]_2$ (0.168 g, 0.25 mmol) in Et_2O (5 mL) at -78 °C. The reaction mixture was allowed to

Dalton Transactions Accepted Manuscript

View Article Online
DOI: 10.1039/C5DT02403J

Published on 23 July 2015. Downloaded by University of California - Santa Barbara on 28/07/2015 05:09:18.

warm to room temperature gradually and was stirred for 12 h. After removal of the volatiles under vacuum, the residue was extracted with toluene and the solution was filtered through Celite. The filtrate was concentrated to *ca.* 2 mL, Et_2O (3 mL) was added and this solution was cooled to -30 °C to yield a dark red crystalline solid (0.194 g, 80%) which was collected by filtration and dried in vacuo. ^{1}H NMR (400 MHz, C_6D_6): δ 7.20 (d, ^3J = 1.4 Hz, 2H, NC*H*CHN$_{(mesityl)}$), 6.74 (s, 2H, aryl-*H*), 6.68 (s, 2H, aryl-*H*), 6.42 (d, ^3J = 1.4 Hz, 2H, NCHC*H*N$_{(mesityl)}$), 4.24 (m, 2H, C*H*$_{(cod)}$), 3.89 (m, 4H, C*H*$_{(cod)}$), 3.55 (m, 2H, C*H*$_{(cod)}$), 2.65–2.31 (m, 8H, C*H*$_{2(cod)}$), 2.10 (s, 12H, *o*-C*H*$_{3(mesityl)}$), 1.91 (s, 6H, *p*-C*H*$_{3(mesityl)}$), 1.85 (m, 4H, C*H*$_{2(cod)}$), 1.64 (m, 4H, C*H*$_{2(cod)}$). ^{13}C{^{1}H} NMR (100 MHz, C_6D_6): δ 171.3 (N*C*N$_{(mesityl)}$), 138.5 (*C*$_{(mesityl)}$), 137.3 (*C*$_{(mesityl)}$), 136.9 (*C*$_{(mesityl)}$), 135.8 (*C*$_{(mesityl)}$), 128.9 (*C*H$_{(mesityl)}$), 128.8 (*C*H$_{(mesityl)}$), 125.5 (N*C*HCHN$_{(mesityl)}$), 122.4 (NCH*C*HN$_{(mesityl)}$), 69.4, 69.0, 65.2 and 59.5 (*C*H$_{(cod)}$), 32.9, 32.7, 32.5 and 32.1 (*C*H$_{2(cod)}$), 21.0 (*p*-*C*H$_{3(mesityl)}$), 20.2 (*o*-*C*H$_{3(mesityl)}$), 18.3 (*o*-*C*H$_{3(mesityl)}$). Anal. Calcd for $C_{40}H_{50}Ir_2N_4$ (%): C, 49.46; H, 5.19; N, 5.77. Found: C, 48.68; H, 5.00; N, 5.72.

From **2**: To a stirred solution of **2** (0.052 g, 0.10 mmol) in THF (5 mL) was added a solution of KHMDS (0.020 g, 0.10 mmol) in THF (2 mL) at -78 °C. The reaction mixture was allowed to warm to room temperature gradually and was stirred for 12 h. After removal of the volatiles under vacuum, the residue was extracted with toluene and the solution was filtered through Celite. The filtrate was evaporated to dryness under reduced pressure to yield a red solid (0.044 g, 91%). ^{1}H NMR analysis of the resulting red solid revealed a *ca.* 40:60 mixture of $\mathbf{3_{H\text{-}H}}$ and $\mathbf{3_{H\text{-}T}}$.

[Ir(cod){μ-$C_3H_2N_2$(Mes)-κC2,κN3}]$_2$ ($\mathbf{3_{H\text{-}T}}$). A solution of $\mathbf{3_{H\text{-}H}}$ (0.048 g, 0.050 mmol) in THF (5 mL) was refluxed for 24 h. After removal of the solvent under vacuum, the residue was washed with pentane (2 × 1 mL) to yield a purple crystalline solid (0.046 g, 96%) which was collected by filtration and dried in vacuo. ^{1}H NMR (300 MHz, C_6D_6): δ 7.02 (d, ^3J = 1.1 Hz, 2H, NC*H*CHN$_{(mesityl)}$), 6.89 (s, 2H, aryl-*H*), 6.77 (s, 2H, aryl-*H*), 6.53 (d, ^3J = 1.1 Hz, 2H, NCHC*H*N$_{(mesityl)}$), 4.32 (m, 2H, C*H*$_{(cod)}$), 3.85 (m, 2H, C*H*$_{(cod)}$), 3.66 (m, 4H, C*H*$_{(cod)}$), 2.67–2.27 (m, 8H, C*H*$_{2(cod)}$), 2.21 (s, 6H, *o*-C*H*$_{3(mesityl)}$), 2.18 (s, 6H, *o*-C*H*$_{3(mesityl)}$), 1.97 (s, 6H, *p*-C*H*$_{3(mesityl)}$), 1.81–1.49 (m, 8H, C*H*$_{2(cod)}$). ^{13}C{^{1}H} NMR (75 MHz, C_6D_6): δ 172.0 (N*C*N$_{(mesityl)}$), 138.3 (*C*$_{(mesityl)}$), 137.2 (*C*$_{(mesityl)}$), 136.8 (*C*$_{(mesityl)}$), 135.0 (*C*$_{(mesityl)}$), 129.3 (*C*H$_{(mesityl)}$), 128.1 (*C*H$_{(mesityl)}$), 125.4 (N*C*HCHN$_{(mesityl)}$), 121.3 (NCH*C*HN$_{(mesityl)}$), 75.7, 73.8, 59.8 and 56.0 (*C*H$_{(cod)}$), 35.4, 33.4, 32.4, 29.4 (*C*H$_{2(cod)}$), 21.1 (*p*-*C*H$_{3(mesityl)}$), 19.2 (*o*-*C*H$_{3(mesityl)}$), 18.2 (*o*-*C*H$_{3(mesityl)}$). Anal. Calcd for $C_{40}H_{50}Ir_2N_4$ (%): C, 49.46; H, 5.19; N, 5.77. Found: C, 49.21; H, 4.96; N, 5.60.

[Ir(CO)$_2${μ-$C_3H_2N_2$(Mes)-κC2,κN3}]$_2$ ($\mathbf{4_{H\text{-}H}}$). A suspension of $\mathbf{3_{H\text{-}H}}$ (0.097 g, 0.100 mmol) in Et_2O (5 mL) was stirred under CO (1 bar) at room temperature and the color turned from red to yellow immediately. The suspension was further stirred for 30 min. After removal of the volatiles under vacuum, the residue was washed with pentane (2 × 1 mL) to yield a yellow crystalline solid which was collected by filtration and dried in vacuo (0.070 g, 81%). ^{1}H NMR (500 MHz, C_6D_6): δ 7.11 (d, ^3J = 1.5 Hz, 2H, NC*H*CHN$_{(mesityl)}$), 6.67 (s, 4H, aryl-*H*), 6.33 (d, ^3J = 1.5 Hz, 2H, NCHC*H*N$_{(mesityl)}$), 2.04 (s, 6H, C*H*$_{3(Mes)}$), 1.96 (s, 6H, C*H*$_{3(Mes)}$), 1.82 (s, 6H, C*H*$_{3(Mes)}$). ^{13}C{^{1}H} NMR (125 MHz, C_6D_6): δ 181.4 (*C*O), 175.5 (*C*O), 172.8 (N*C*N$_{(mesityl)}$), 138.7 (*C*$_{(mesityl)}$), 136.8 (*C*$_{(mesityl)}$), 136.4 (*C*$_{(mesityl)}$), 136.1 (*C*$_{(mesityl)}$), 131.4 (N*C*HCHN$_{(mesityl)}$), 129.4 (*C*H$_{(mesityl)}$), 129.0 (*C*H$_{(mesityl)}$), 123.0 ((NCH*C*HN$_{(mesityl)}$)), 21.0 (*C*H$_{3(mesityl)}$), 19.6 (*C*H$_{3(mesityl)}$), 18.1 (*C*H$_{3(mesityl)}$). IR (pure, orbit diamond): ν_{CO} = 2060, 2037, 1954 cm^{-1}. Anal. Calcd for $C_{28}H_{26}Ir_2N_4O_4$ (%): C, 38.79; H, 3.02; N, 6.46. Found: C, 38.53; H, 3.15; N, 6.29.

[Ir(CO)$_2${μ-$C_3H_2N_2$(Mes)-κC2,κN3}]$_2$ ($\mathbf{4_{H\text{-}T}}$). A procedure similar to that used for the synthesis of $\mathbf{4_{H\text{-}H}}$ but starting from $\mathbf{3_{H\text{-}T}}$ yielded a brown solid (0.065 g, 75%). ^{1}H NMR (300 MHz, C_6D_6): δ 6.95 (d, ^3J = 1.6 Hz, 2H, NC*H*CHN$_{(mesityl)}$), 6.79 (s, 2H, aryl-*H*), 6.77 (s, 2H, aryl-*H*), 6.41 (d, ^3J = 1.6 Hz, 2H, NCHC*H*N$_{(mesityl)}$), 2.09 (s, 6H, *p*-C*H*$_{3(mesityl)}$), 1.95 (s, 12H, *o*-C*H*$_{3(mesityl)}$). ^{13}C{^{1}H} NMR (75 MHz, C_6D_6): δ 183.7 (*C*O), 175.7 (*C*O), 175.1 (N*C*N$_{(mesityl)}$), 138.7 (*C*$_{(mesityl)}$), 136.5 (*C*$_{(mesityl)}$), 135.6 (*C*$_{(mesityl)}$), 130.5 (N*C*HCHN$_{(mesityl)}$), 129.4 (*C*H$_{(mesityl)}$), 129.3 (*C*H$_{(mesityl)}$), 122.1 (NCH*C*HN$_{(mesityl)}$), 21.1 (*p*-*C*H$_{3(mesityl)}$), 18.7 (*o*-*C*H$_{3(mesityl)}$), 18.0 (*o*-*C*H$_{3(mesityl)}$). IR (pure, orbit diamond): ν_{CO} = 2059, 2041, 1968 cm^{-1}. Anal. Calcd for $C_{28}H_{26}Ir_2N_4O_4$ (%): C, 38.79; H, 3.02; N, 6.46. Found: C, 38.42; H, 3.22; N, 6.63.

[Ir(CO)(PMe$_3$){μ-$C_3H_2N_2$(Mes)-κC2,κN3}]$_2$ (5). This complex can be synthesized by reaction of either $\mathbf{4_{H\text{-}T}}$ or $\mathbf{4_{H\text{-}H}}$ with 2.0 equiv. of trimethylphosphine.

From $\mathbf{4_{H\text{-}T}}$: To a solution of $\mathbf{4_{H\text{-}T}}$ (0.043 g, 0.05 mmol) in toluene (5 mL) was added a solution of PMe_3 (0.1 M in Et_2O, 1.0 mL, 0.1 mmol). The mixture was stirred for 4 h and the initially yellow solution became red. After removal of the volatiles under vacuum, the residue was washed with pentane (2 × 1 mL) to yield a red crystalline solid which was collected by filtration and dried in vacuo (0.045 g, 93%). ^{1}H NMR (500 MHz, C_6D_6): δ 6.90 (s, 2H, aryl-*H*), 6.89 (d, ^3J = 1.0 Hz, 2H, NC*H*CHN$_{(mesityl)}$), 6.77 (s, 2H, aryl-*H*), 6.68 (apparent t, $^3J_{H\text{-}H}$, $^5J_{H\text{-}P}$ = 1.0 Hz, 2H, NCHC*H*N$_{(mesityl)}$), 2.28 (s, 6H, *o*-C*H*$_{3(mesityl)}$), 2.18 (s, 6H, *o*-C*H*$_{3(mesityl)}$), 2.08 (s, 6H, *p*-C*H*$_{3(mesityl)}$), 1.13 (d, $^2J_{H\text{-}P}$ = 8.7 Hz, 18H, PC*H*$_3$). ^{31}P{^{1}H} NMR (121.5 MHz, C_6D_6): δ -24.1. ^{13}C{^{1}H} NMR (125 MHz, C_6D_6): δ 181.4 (d, $^2J_{C\text{-}P}$ = 10.0 Hz, *C*O), 177.1 (d, $^2J_{C\text{-}P}$ = 112.0 Hz, N*C*N$_{(mesityl)}$), 138.3 (*C*$_{(mesityl)}$), 137.5 (*C*$_{(mesityl)}$), 136.7 (*C*$_{(mesityl)}$), 135.5 (*C*$_{(mesityl)}$), 129.4 (*C*H$_{(mesityl)}$), 128.9 (*C*H$_{(mesityl)}$), 128.0 (d, $^4J_{C\text{-}P}$ = 5.2 Hz, N*C*HCHN$_{(mesityl)}$), 120.1 (d, $^4J_{C\text{-}P}$ = 2.0 Hz, NCH*C*HN$_{(mesityl)}$), 21.1 (*p*-*C*H$_{3(mesityl)}$), 18.9 (*o*-*C*H$_{3(mesityl)}$), 18.3 (*o*-*C*H$_{3(mesityl)}$), 17.0 (d, $^1J_{C\text{-}P}$ = 31.6 Hz, P*C*H$_3$). IR (pure, orbit diamond): ν_{CO} = 2000, 1911 cm^{-1}. Anal. Calcd for $C_{32}H_{44}Ir_2N_4O_2P_2$ (%): C, 39.91; H, 4.60; N, 5.82. Found: C, 39.88; H, 4.70; N, 5.75.

From $\mathbf{4_{H\text{-}H}}$: A procedure similar to that used with $\mathbf{4_{H\text{-}T}}$ was employed to yield the same red crystalline solid (0.046 g, 96%).

[Ir$_2$(CO)$_2$(PMe$_3$)$_2$(Me)I{μ-$C_3H_2N_2$(Mes)-κC2,κN3}$_2$] (6). To a stirred solution of **5** (0.030 g, 0.032 mmol) in THF (5 mL) was added dropwise over 2 min a solution of MeI (0.1 M in

Dalton Transactions Accepted Manuscript

View Article Online
DOI: 10.1039/C5DT02403J

Published on 23 July 2015. Downloaded by University of California - Santa Barbara on 28/07/2015 05:09:18.

Et_2O, 0.4 mL, 0.04 mmol) and the mixture was stirred for 5 min. Concentration of the solution under vacuum to 2 mL followed by addition of pentane (5 mL) afforded the product as a yellow powder (0.032 g, 90%). ^{1}H NMR (500 MHz, C_6D_6): δ 7.87 (d, ^3J = 1.2 Hz, 1H, NC*H*CHN$_{(mesityl)}$), 6.97 (s, 1H, aryl-*H*), 6.89 (s, 1H, aryl-*H*), 6.75 (s, 2H, aryl-*H*), 6.73 (d, ^3J = 1.2 Hz, 1H, NC*H*CHN$_{(mesityl)}$), 6.19 (t, $J_{H\text{-}H}$, $J_{H\text{-}P}$ = 1.2 Hz, 1H, NCHC*H*N$_{(mesityl)}$), 6.04 (t, $J_{H\text{-}H}$, $J_{H\text{-}P}$ = 1.2 Hz, 1H, NCHC*H*N$_{(mesityl)}$), 2.26 (s, 3H, C*H*$_{3(mesityl)}$), 2.22 (s, 3H, C*H*$_{3(mesityl)}$), 2.15 (s, 3H, C*H*$_{3(mesityl)}$), 2.12 (s, 3H, C*H*$_{3(mesityl)}$), 1.96 (s, 3H, C*H*$_{3(mesityl)}$), 1.74 (s, 3H, C*H*$_{3(mesityl)}$), 1.51 (d, $^2J_{H\text{-}P}$ = 9.6 Hz, 9H, PC*H*$_3$), 1.02 (d, $^2J_{H\text{-}P}$ = 9.6 Hz, 9H, PC*H*$_3$), 0.71 (d, $^3J_{H\text{-}P}$ = 5.7 Hz, 3H, IrC*H*$_3$). ^{31}P{^{1}H} NMR (121.5 MHz, C_6D_6): δ -46.6, -48.9. ^{13}C{^{1}H} NMR (125 MHz, C_6D_6): δ 181.5 (d, $^2J_{C\text{-}P}$ = 10.5 Hz, *C*O), 180.0 (d, $^2J_{C\text{-}P}$ = 9.6 Hz, *C*O), 142.8 (d, $^2J_{C\text{-}P}$ = 136.7 Hz, N*C*N$_{(mesityl)}$), 140.8 (d, $^2J_{C\text{-}P}$ = 141.1 Hz, N*C*N$_{(mesityl)}$), 138.2, 138.1, 137.9, 136.8, 136.7, 136.5, 135.2 and 135.0 (*C*$_{(mesityl)}$), 131.9 (d, $^4J_{C\text{-}P}$ = 4.6 Hz, N*C*HCHN$_{(mesityl)}$), 129.8, 129.1, 129.0 and 128.9 (*C*H$_{(mesityl)}$), 122.2 (d, $^4J_{C\text{-}P}$ = 3.8 Hz, NCH*C*HN$_{(mesityl)}$), 121.5 (d, $^4J_{C\text{-}P}$ = 3.8 Hz, N*C*HCHN$_{(mesityl)}$), 121.0 (d, $^4J_{C\text{-}P}$ = 3.7 Hz, NCH*C*HN$_{(mesityl)}$), 21.4 (*C*H$_{3(mesityl)}$), 21.2 (*C*H$_{3(mesityl)}$), 18.7 (*C*H$_{3(mesityl)}$), 18.6 (d, $^1J_{C\text{-}P}$ = 34.9 Hz, P*C*H$_3$), 18.4 (*C*H$_{3(mesityl)}$), 17.8 (*C*H$_{3(mesityl)}$), 17.3 (*C*H$_{3(mesityl)}$), 14.8 (d, $^1J_{C\text{-}P}$ = 33.5 Hz, P*C*H$_3$), -31.8 (d, $^2J_{C\text{-}P}$ = 2.3 Hz, Ir*C*H$_3$). IR (pure, orbit diamond): ν_{CO} = 2019, 1952 cm^{-1}. Anal. Calcd for $C_{33}H_{47}Ir_2N_4O_2P_2$ (%): C, 35.87; H, 4.29; N, 5.07. Found: C, 35.33; H, 4.02; N, 5.21.

[Ir(C$_2$H$_4$)$_2${μ-C$_3$H$_2$N$_2$(Mes)-κC2,κN3}]$_2$ (7). To a stirred solution of **1a** (0.100 g, 0.52 mmol) in Et_2O (10 mL) was added a solution of [Ir(C$_2$H$_4$)$_2$(μ-Cl)]$_2$ (0.142 g, 0.25 mmol) in Et_2O (5 mL) at -78 °C. The reaction mixture was allowed to warm to room temperature gradually and was further stirred for 4 h. After removal of volatiles in vacuo, the residue was extracted with toluene and the solution was filtered through Celite. After evaporation of the toluene, the solid was washed with pentane (2 × 1 mL) at 0 °C and dried in vacuo to yield a blue solid, which was stored at -30 °C (0.167 g, 77%). ^{1}H NMR (600 MHz, C_6D_6): δ 7.09 (d, ^3J = 1.5 Hz, 2H, NC*H*CHN$_{(mesityl)}$), 6.80 (s, 2H, aryl-*H*), 6.74 (s, 2H, aryl-*H*), 6.49 (d, ^3J = 1.5 Hz, 2H, NCHC*H*N$_{(mesityl)}$), 3.13 (broad B part of an AA'BB' spin system, 4H, C*H*$_{2(ethylene)}$) and 2.89 (broad A part of an AA'BB' spin system, 4H, C*H*$_{2(ethylene)}$), 2.63 (B part of an AA'BB' spin system with |N| ≈ 8.2 Hz, 4H, C*H*$_{2(ethylene)}$) and 2.36 (A part of an AA'BB' spin system with |N| ≈ 8.2 Hz, 4H, C*H*$_{2(ethylene)}$), 2.11 (s, 6H, *o*-C*H*$_{3(mesityl)}$), 2.08 (s, 6H, *o*-C*H*$_{3(mesityl)}$), 1.97 (s, 6H, *p*-C*H*$_{3(mesityl)}$). ^{13}C{^{1}H} NMR (150 MHz, C_6D_6): δ 171.5 (N*C*N$_{(mesityl)}$), 137.8 (*C*$_{(mesityl)}$), 137.5 (*C*$_{(mesityl)}$), 136.7 (*C*$_{(mesityl)}$), 134.8 (*C*$_{(mesityl)}$), 129.7 (*C*H$_{(mesityl)}$), and 128.8 (*C*H$_{(mesityl)}$), 124.6 (N*C*HCHN$_{(mesityl)}$), 122.0 (NCH*C*HN$_{(mesityl)}$), 60.5 (*C*H$_{2(ethylene)}$), 42.3 (*C*H$_{2(ethylene)}$), 21.5 (*p*-*C*H$_{3(mesityl)}$), 19.0 (*o*-*C*H$_{3(mesityl)}$), 18.1 (*o*-*C*H$_{3(mesityl)}$). Calcd for $C_{32}H_{42}Ir_2N_4$ (%): C, 44.32; H, 4.88; N, 6.46. Found: C, 43.88; H, 4.95; N, 6.73.

[Rh(cod){μ-C$_3$H$_2$N$_2$(Mes)-κC2,κN3}]$_2$ (8). A procedure similar to that used for the synthesis of **3$_{H\text{-}H}$** was used but starting from [Rh(cod)(μ-Cl)]$_2$. Treatment of **1a** (0.100 g, 0.52 mmol) with [Rh(cod)(μ-Cl)]$_2$ (0.123 g, 0.25 mmol) afforded an orange solid (0.168 g, 85%). ^{1}H NMR (500 MHz, C_6D_6): δ 6.96 (an overlap of two s, 4H, NC*H*CHN$_{(mesityl)}$ and aryl-*H*), 6.77 (s, 2H, aryl-*H*), 6.51 (s, 2H, NCHC*H*N$_{(mesityl)}$), 4.72 (m, 2H, C*H*$_{(cod)}$), 4.48 (m, 2H, C*H*$_{(cod)}$), 4.09 (m, 2H, C*H*$_{(cod)}$), 3.76 (m, 2H, C*H*$_{(cod)}$), 2.73–2.55 (m, 4H, C*H*$_{2(cod)}$), 2.31 (s, 6H, *o*-C*H*$_{3(mesityl)}$), 2.20 (s, 6H, *o*-C*H*$_{3(mesityl)}$), 2.09–1.96 (m, 8H, C*H*$_{2(cod)}$), 1.94 (s, 6H, *p*-C*H*$_{3(mesityl)}$), 1.86–1.77 (m, 4H, C*H*$_{2(cod)}$). ^{13}C{^{1}H} NMR (125 MHz, C_6D_6): δ 176.2 (d, $^1J_{C\text{-}Rh}$ = 50.4 Hz, N*C*N$_{(mesityl)}$), 138.8 (*C*$_{(mesityl)}$), 137.2 (*C*$_{(mesityl)}$), 137.0 (*C*$_{(mesityl)}$), 135.1 (*C*$_{(mesityl)}$), 129.3 (*C*H$_{(mesityl)}$), 128.6 (*C*H$_{(mesityl)}$), 126.8 (N*C*HCHN$_{(mesityl)}$), 120.3 (NCH*C*HN$_{(mesityl)}$), 90.3 (d, $^1J_{C\text{-}Rh}$ = 8.4 Hz, *C*H$_{(cod)}$), 89.3 (d, $^1J_{C\text{-}Rh}$ = 7.3 Hz, *C*H$_{(cod)}$), 79.2 (d, $^1J_{C\text{-}Rh}$ = 12.9 Hz, *C*H$_{(cod)}$), 72.0 (d, $^1J_{C\text{-}Rh}$ = 11.9 Hz, *C*H$_{(cod)}$), 33.4, 33.3, 30.7 and 29.6 (*C*H$_{2(cod)}$), 21.1 (*p*-*C*H$_{3(mesityl)}$), 19.5 (*o*-*C*H$_{3(mesityl)}$), 18.2 (*o*-*C*H$_{3(mesityl)}$). Calcd for $C_{40}H_{50}Rh_2N_4$ (%): C, 60.61; H, 6.36; N, 7.07. Found: C, 60.13; H, 6.48; N, 7.32.

[Rh(C$_2$H$_4$)$_2${μ-C$_3$H$_2$N$_2$(Dipp)-κC2,κN3}]$_2$ (9). To a stirred solution of **1b** (0.120 g, 0.51 mmol) in Et_2O (10 mL) was added a solution of [Rh(C$_2$H$_4$)$_2$(μ-Cl)]$_2$ (0.085 g, 0.25 mmol) in Et_2O (5 mL) at -78 °C. The reaction mixture was allowed to warm to room temperature gradually and was further stirred for 4 h. After removal of the volatiles under vacuum, the residue was extracted with *n*-hexane and the solution was filtered through Celite. The filtrate was concentrated to ca. 4 mL under reduced presssure and then was cooled to -30 °C in an ethylene atmosphere to obtain purple crystals, which were stored at -30 °C (0.135 g, 70%). ^{1}H NMR (400 MHz, C_6D_6): δ 7.28 (d, ^3J = 4.4 Hz, 4H, *m*-aryl-*H*), 7.08 (t, ^3J = 4.4 Hz, 2H, *p*-aryl-*H*), 7.02 (s, 2H, NC*H*CHN$_{(Dipp)}$), 6.64 (s, 2H, NCHC*H*N$_{(Dipp)}$), 3.65 (B part of a broad poorly resolved AA'BB' spin system, 4H, C*H*$_{2(ethylene)}$) and 3.58 (A part of a broad poorly resolved AA'BB' spin system, 4H, C*H*$_{2(ethylene)}$), 3.25 (sept, ^3J = 6.8 Hz, 2H, C*H*(CH$_3$)$_2$), 2.86 (B part of an AA'BB' spin system with |N| ≈ 7.5 Hz and poorly resolved Rhodium coupling, 4H, C*H*$_{2(ethylene)}$) and 2.62 (A part of an AA'BB' spin system with |N| ≈ 7.5 Hz and poorly resolved Rhodium coupling, 4H, C*H*$_{2(ethylene)}$), 2.48 (sept, ^3J = 6.8 Hz, 2H, C*H*(CH$_3$)$_2$), 1.73 (d, ^3J = 6.8 Hz, 6H, CH(C*H*$_3$)$_2$), 1.16 (d, ^3J = 6.8 Hz, 6H, CH(C*H*$_3$)$_2$), 1.06 (d, ^3J = 6.8 Hz, 6H, CH(C*H*$_3$)$_2$), 0.80 (d, ^3J = 6.8 Hz, 6H, CH(C*H*$_3$)$_2$). ^{13}C{^{1}H} NMR (100 MHz, C_6D_6): δ 175.1 (d, $^1J_{C\text{-}Rh}$ = 49.0 Hz, N*C*N$_{(Dipp)}$), 147.1 (*C*$_{(Dipp)}$), 146.1 (*C*$_{(Dipp)}$), 137.8 (*C*$_{(Dipp)}$), 128.9 (*C*H$_{(Dipp)}$), 125.9 (N*C*HCHN$_{(Dipp)}$), 124.1 (*C*H$_{(Dipp)}$), 123.8 (*C*H$_{(Dipp)}$), 122.8 (NCH*C*HN$_{(Dipp)}$), 78.7 (d, $^1J_{C\text{-}Rh}$ = 6.6 Hz, *C*H$_{2(ethylene)}$), 58.0 (d, $^1J_{C\text{-}Rh}$ = 12.1 Hz, *C*H$_{2(ethylene)}$), 28.8 (*C*H(CH$_3$)$_2$), 28.3(*C*H(CH$_3$)$_2$), 26.3, 24.9, 24.2 and 23.4 (CH(*C*H$_3$)$_2$). Calcd for $C_{38}H_{54}Rh_2N_4$ (%): C, 59.07; H, 7.04; N, 7.25. Found: C, 58.63; H, 6.87; N, 7.42.

Catalytic transfer dehydrogenation of cyclooctane.

In a preliminary investigation, a red suspension of complex **3$_{H\text{-}T}$** (9.7 mg, 0.010 mmol) in a mixture of COA (4.0 mL, 30.3 mmol) and TBE (0.40 mL, 3.1 mmol), in a sealed tube under argon, was heated at 200 ºC for 10 h (Table 3, entry 1). Gas chromatographic (GC) analysis of the products indicated 0.15% of the cyclooctane was converted to *cis*-cyclooctene

Dalton Transactions Accepted Manuscript

View Article Online
DOI: 10.1039/C5DT02403J

Published on 23 July 2015. Downloaded by University of California - Santa Barbara on 28/07/2015 05:09:18.

at a turnover frequency (TOF) 0.46 h^{-1}. The formation of TBA, confirmed by GC and ^1H NMR analysis, also indicated that the transfer dehydrogenation reaction did occur. When complex $\mathbf{4_{H\text{-}T}}$ was used as the precatalyst under the same reaction conditions (Table 3, entry 2), no catalytic activity was observed. In the catalytic reaction using complex **5** (Table 3, entry 3), in which two CO ligands of complex **4** are replaced by two molecules of PMe_3, GC analysis of the products indicated that 0.19% of the cyclooctane was converted to *cis*-cyclooctene at a TOF of 0.58 h^{-1}. Better results were obtained with complex **7** where 2.06% of the cyclooctane was converted to *cis*-cyclooctene at a TOF of 6.24 h^{-1}.

X-ray Data Collection, Structure Solution, and Refinement for All Compounds.

Suitable crystals for the X-ray analysis of all compounds were obtained as described above. Data for $\mathbf{3_{H\text{-}H}}$, $\mathbf{3_{H\text{-}T}}$ and **8** were collected on an APEX-II CCD (graphite-monochromated Mo-Kα radiation, λ = 0.71073 Å) at 173(2) K and data for **9** were collected on a Kappa CCD diffractometer (graphite-monochromated Mo-Kα radiation, λ = 0.71073 Å) at 173(2) K. Crystallographic and experimental details for these structures are summarized in Table S1 (see ESI). The structures were solved by direct methods (SHELXS-97[28]) and refined by full-matrix least-squares procedures (based on F^2, SHELXL-97) with anisotropic thermal parameters for all the non-hydrogen atoms. The hydrogen atoms were introduced into the geometrically calculated positions (SHELXS-97 procedures). The SQUEEZE instruction in PLATON was applied for **9** and the residual electron density was assigned to half a molecule of disordered *n*-hexane. In **9**, one methyl group (C11) was found disordered over two positions.

Electrochemistry

All compounds were studied in CH_2Cl_2 + 0.1 mM [*n*-Bu_4N]PF_6. [*n*-Bu_4N]PF_6 (Fluka, electrochemical grade) and CH_2Cl_2 (Merck, UVasol®) were used as received. The electrochemical measurements were carried out at room temperature (20 °C) in CH_2Cl_2 containing 0.1 M [*n*-Bu_4N]PF_6 in a classical three-electrode cell. The electrolyte was degassed by bubbling argon through the solution for at least 5 min, and an argon flow was kept over the solution during measurements. The electrochemical cell was connected to a computerized multipurpose electrochemical device (Autolab, Eco Chemie BV, The Netherlands) controlled by a GPES software (v. 4.7) running on a PC computer. The working electrode was a glassy carbon (GC) disk electrode (diameter: 3 mm), used either motionless for cyclic voltammetry (100 mV s^{-1} to 10 V s^{-1}) or as a rotating disk electrode. The auxiliary electrode was a Pt wire, and the pseudo reference electrode a Pt wire. All potentials are given *vs*. Fc^+/Fc used as internal reference in agreement with the IUPAC recommendation[29] and are uncorrected from ohmic drop.

The number of exchanged electrons for the first oxidation step was determined by exhaustive electrolysis. Prior to electrolysis, the corresponding mixtures were stirred and degassed by bubbling argon through the solution for 10 min. Then, the desired working potential was applied. During anodic oxidation, the electrolyzed solution was continuously stirred and maintained under argon. Coulometric measurements were performed in a standard 40 mL cell. The working and the auxiliary electrodes were a platinum wire (o.d. 0.8 mm) of 15 cm length. For the controlled-potential electrolysis, the anodic and cathodic compartments were separated by a fritted-glass disk to prevent diffusion of the electrogenerated species.

The reference electrode was a saturated calomel electrode (SCE) that was electrically connected to the studied solution by a junction bridge filled with the corresponding solvent-supporting electrolyte solution.

Spectroelectrochemical experiments were carried out as described elsewhere,[30] using a Zeiss MCS 601 UV–vis–NIR diode array spectrometer.

UV-visible-NIR spectroscopy

UV–Vis absorption spectra have been recorded for 4.41 10^{-5} mol L^{-1} ($\mathbf{3_{H\text{-}T}}$) and 8.07 10^{-5} mol L^{-1} (**8**) solutions in CH_2Cl_2 on a Perkin–Elmer Lambda 35 spectrophotometer in quartz cells (1 cm). The UV-visible-NIR absorption spectroscopic measurements were performed in CH_2Cl_2. The optical absorption spectrum of $\mathbf{3_{H\text{-}T}}$ (Fig. S1 in ESI) was characterised by a band in the visible domain around 525 nm ($\varepsilon_{525\ nm}$ = 3648 dm^3 mol^{-1} cm^{-1}). In the case of the **8** (Fig. S3 in ESI), the band was observed at 476 nm ($\varepsilon_{476\ nm}$ = 4585 dm^3 mol^{-1} cm^{-1}).

EPR experiments

EPR spectra were recorded with an EMX spectrometer (Bruker) operating at X-band and equipped with a standard HSN cavity and a variable temperature attachment. Computer simulations of the EPR spectra were performed with the help of Easy Spin software.[31]

DFT calculations

All theoretical calculations were performed with the ORCA program package.[32] Geometry optimization was carried out using the GGA functional BP86[33] and by taking advantage of the resolution of the identity (RI) approximation in the Split-RI-J[34] variant with the appropriate Coulomb fitting sets.[35] Increased integration grids (Grid4 and GridX4 in ORCA convention) and tight SCF convergence criteria were used. Solvent effects were accounted for according to the experimental conditions. For that purpose, we used the CH_2Cl_2 (□□= 9.08) solvent within the framework of the conductor like screening (COSMO) dielectric continuum approach.[36] Electronic structures were obtained from single-point calculations using the B3LYP[37] functional. Scalar relativistic effects were included using the scalar relativisitc zero-order regular approximation (ZORA)[38] and the scalar

Dalton Transactions Accepted Manuscript

View Article Online
DOI: 10.1039/C5DT02403J

relativistically recontracted (SARC)[39] version of the def2-TZVP(-f) basis set together with the decontracted def2-TZVP/J Coulomb fitting basis sets for all atoms. Spin density and molecular orbitals were plotted using the orca_plot utility program and visualized with Chemcraft[40] software.

Acknowledgements

The USIAS, CNRS, UdS, Région Alsace and Communauté Urbaine de Strasbourg are gratefully acknowledged for the award of fellowships and a Gutenberg Excellence Chair (2010–11) to AAD and support. We also thank the ucFRC (www.icfrc.fr) for support and the China Scholarship Council for a PhD grant to F. H., and the Service de Radiocristallographie (Institut de Chimie, Strasbourg) for the determination of the crystal structures.

Notes and references

1. (a) A. J. Arduengo, III, R. L. Harlow and M. Kline, *J. Am. Chem. Soc.*, 1991, **113**, 361; (b) A. J. Arduengo, H. V. R. Dias, R. L. Harlow and M. Kline, *J. Am. Chem. Soc.*, 1992, **114**, 5530.
2. (a) M. Melaimi, M. Soleilhavoup and G. Bertrand, *Angew. Chem. Int. Ed.*, 2010, **49**, 8810; (b) P. de Frémont, N. Marion and S. P. Nolan, *Coord. Chem. Rev.*, 2009, **253**, 862; (c) F. E. Hahn and M. C. Jahnke, *Angew. Chem. Int. Ed.*, 2008, **47**, 3122; (d) D. Bourissou, O. Guerret, F. P. Gabbaï and G. Bertrand, *Chem. Rev.*, 2000, **100**, 39.
3. (a) S. Kuwata and T. Ikariya, *Chem.–Eur. J.*, 2011, **17**, 3542; (b) S. Kuwata and T. Ikariya, *Chem. Commun.*, 2014, **50**, 14290.
4. F. E. Hahn, *ChemCatChem*, 2013, **5**, 419.
5. (a) C.-H. Hsieh, R. Pulukkody and M. Y. Darensbourg, *Chem. Commun.*, 2013, **49**, 9326; (b) D. Brackemeyer, A. Hervé, C. Schulte to Brinke, M. C. Jahnke and F. E. Hahn, *J. Am. Chem. Soc.*, 2014, **136**, 7841.
6. (a) F. E. Hahn, V. Langenhahn, T. Lügger, T. Pape and D. Le Van, *Angew. Chem. Int. Ed.*, 2005, **44**, 3759; (b) F. E. Hahn, V. Langenhahn and T. Pape, *Chem. Commun.*, 2005, 5390; (c) J. Ruiz, G. García, M. E. G. Mosquera, B. F. Perandones, M. P. Gonzalo and M. Vivanco, *J. Am. Chem. Soc.*, 2005, **127**, 8584.
7. (a) G. E. Dobereiner, C. A. Chamberlin, N. D. Schley and R. H. Crabtree, *Organometallics*, 2010, **29**, 5728; (b) P. C. Kunz, C. Wetzel, S. Kogel, M. U. Kassack and B. Spingler, *Dalton Trans.*, 2011, **40**, 35.
8. (a) T. Kösterke, T. Pape and F. E. Hahn, *J. Am. Chem. Soc.*, 2011, **133**, 2112; (b) T. Kösterke, J. Kösters, E.-U. Würthwein, C. Mück-Lichtenfeld, C. Schulte to Brinke, F. Lahoz and F. E. Hahn, *Chem.–Eur. J.*, 2012, **18**, 14594; (c) R. Das, C. G. Daniliuc and F. E. Hahn, *Angew. Chem. Int. Ed.*, 2014, **53**, 1163; (d) R. Das, A. Hepp, C. G. Daniliuc and F. E. Hahn, *Organometallics*, 2014, **33**, 6975.
9. F. He, P. Braunstein, M. Wesolek and A. A. Danopoulos, *Chem. Commun.*, 2015, **51**, 2814.
10. (a) C. Hill, F. Bosold, K. Harms, J. C. W. Lohrenz, M. Marsch, M. Schmieczek and G. Boche, *Chem. Ber.*, 1997, **130**, 1201; (b) C. Hilf, F. Bosold, K. Harms, M. Marsch and G. Boche, *Chem. Ber.*, 1997, **130**, 1213.
11. A. P. Marchenko, H. N. Koidan, I. I. Pervak, A. N. Huryeva, E. V. Zarudnitskii, A. A. Tolmachev and A. N. Kostyuk, *Tetrahedron Lett.*, 2012, **53**, 494.
12. (a) K. A. Beveridge, G. W. Bushnell, K. R. Dixon, D. T. Eadie, S. R. Stobart, J. L. Atwood and M. J. Zaworotko, *J. Am. Chem. Soc.*, 1982, **104**, 920; (b) A. W. Coleman, D. T. Eadie, S. R. Stobart, M. J. Zaworotko and J. L. Atwood, *J. Am. Chem. Soc.*, 1982, **104**, 922; (c) G. W. Bushnell, D. O. K. Fjeldsted, S. R. Stobart and M. J. Zaworotko, *J. Chem. Soc. Chem. Commun.*, 1983, 580; (d) J. L. Atwood, K. A. Beveridge, G. W. Bushnell, K. R. Dixon, D. T. Eadie, S. R. Stobart and M. J. Zaworotko, *Inorg. Chem.*, 1984, **23**, 4050; (e) G. W. Bushnell, M. J. Decker, D. T. Eadie, S. R. Stobart, R. Vefghi, J. L. Atwood and M. J. Zaworotko, *Organometallics*, 1985, **4**, 2106; (f) D. O. K. Fjeldsted, S. R. Stobart and M. J. Zaworotko, *J. Am. Chem. Soc.*, 1985, **107**, 8258; (g) G. W. Bushnell, D. O. K. Fjeldsted, S. R. Stobart and J. Wang, *Organometallics*, 1996, **15**, 3785; (h) M. A. Arthurs, J. Bickerton, S. R. Stobart and J. Wang, *Organometallics*, 1998, **17**, 2743.
13. (a) K. A. Beveridge, G. W. Bushnell, S. R. Stobart, J. L. Atwood and M. J. Zaworotko, *Organometallics*, 1983, **2**, 1447; (b) G. W. Bushnell, D. O. K. Fjeldsted, S. R. Stobart, M. J. Zaworotko, S. A. R. Knox and K. A. MacPherson, *Organometallics*, 1985, **4**, 1107; (c) Y. Yuan, M. V. Jiménez, E. Sola, F. J. Lahoz and L. A. Oro, *J. Am. Chem. Soc.*, 2002, **124**, 752.
14. (a) R. D. Brost and S. R. Stobart, *Inorg. Chem.*, 1989, **28**, 4307; (b) R. D. Brost, D. O. K. Fjeldsted and S. R. Stobart, *J. Chem. Soc. Chem. Commun.*, 1989, 488.
15. D. L. Lichtenberger, A. S. Copenhaver, H. B. Gray, J. L. Marshall and M. D. Hopkins, *Inorg. Chem.*, 1988, **27**, 4488.
16. (a) J. Müller, C. Hänsch and J. Pickardt, *J. Organomet. Chem.*, 1983, **259**, C21; (b) F. Bonati, L. A. Oro, M. T. Pinillos, C. Tejel and B. Bovio, *J. Organomet. Chem.*, 1994, **465**, 267.
17. J. Müller and R. Stock, *Angew. Chem. Int. Ed. Engl.*, 1983, **22**, 993.
18. R. Cramer, J. B. Kline and J. D. Roberts, *J. Am. Chem. Soc.*, 1969, **91**, 2519.
19. The AA'BB' pattern can be treated with a good approximation as an AA'XX'. See: H. Günther, *NMR Spectroscopy: Basic Principles, Concepts, and Applications in Chemistry*, 3rd edn., Wiley-VCH Verlag GmbH & Co, Weinheim, Germany, 2013.
20. (a) W. Kaim, S. Berger, S. Greulich, R. Reinhardt and J. Fiedler, *J. Organomet. Chem.*, 1999, **582**, 153; (b) S. Frantz, R. Reinhardt, S. Greulich, M. Wanner, J. Fiedler, C. Duboc-Toia and W. Kaim, *Dalton Trans.*, 2003, 3370; (c) W. Kaim and J. Fiedler, *Chem. Soc. Rev.*, 2009, **38**, 3373.
21. N. S. Hush, *Electrochim. Acta*, 1968, **13**, 1005.
22. M. B. Robin and P. Day, in *Advances in Inorganic Chemistry and Radiochemistry*, eds. H. J. Emeléus and A. G. Sharpe, Academic Press, 1968, vol. Volume 10, pp. 247.
23. (a) V. Kasack, W. Kaim, H. Binder, J. Jordanov and E. Roth, *Inorg. Chem.*, 1995, **34**, 1924; (b) S. Patra, B. Sarkar, S. Ghumaan, J. Fiedler, W. Kaim and G. K. Lahiri, *Dalton Trans.*, 2004, 754.
24. J. Choi, A. H. R. MacArthur, M. Brookhart and A. S. Goldman, *Chem. Rev.*, 2011, **111**, 1761.
25. I. Göttker-Schnetmann, P. White and M. Brookhart, *J. Am. Chem. Soc.*, 2004, **126**, 1804.
26. G. Giordano, R. H. Crabtree, R. M. Heintz, D. Forster and D. E. Morris, *Inorg. Synth.*, 1990, **28**, 88.
27. R. Cramer, *Inorg. Chem.*, 1962, **1**, 722.

Published on 23 July 2015. Downloaded by University of California - Santa Barbara on 28/07/2015 05:09:18.

Dalton Transactions Accepted Manuscript

View Article Online
DOI: 10.1039/C5DT02403J

28. G. M. Sheldrick, *SHELXL-97, Program for crystal structure refinement*, University of Göttingen, Göttingen, Germany, 1997.
29. G. Gritzner and J. Kuta, *Pure Appl. Chem.*, 1984, **56**, 461.
30. J. Bley-Escrich, J.-P. Gisselbrecht, E. Vogel and M. Gross, *Eur. J. Inorg. Chem.*, 2002, 2829.
31. S. Stoll and A. Schweiger, *J. Magn. Reson.*, 2006, **178**, 42.
32. F. Neese, *WIREs Comput Mol Sci*, 2012, **2**, 73.
33. (a) J. P. Perdew, *Phys. Rev. B*, 1986, **33**, 8822; (b) J. P. Perdew, *Phys. Rev. B*, 1986, **34**, 7406; (c) A. D. Becke, *Phys. Rev. A*, 1988, **38**, 3098.
34. F. Neese, *J. Comput. Chem.*, 2003, **24**, 1740.
35. F. Weigend, *Phys. Chem. Chem. Phys.*, 2006, **8**, 1057.
36. A. Klamt and G. Schuurmann, *J. Chem. Soc., Perkin Trans. 2*, 1993, 799.
37. (a) A. D. Becke, *J. Chem. Phys.*, 1993, **98**, 1372; (b) C. Lee, W. Yang and R. G. Parr, *Phys. Rev. B*, 1988, **37**, 785.
38. (a) C. Chang, M. Pelissier and P. Durand, *Phys. Scr.*, 1986, **34**, 394; (b) J.-L. Heully, I. Lindgren, E. Lindroth, S. Lundqvist and A.-M. Martensson-Pendrill, *J. Phys. B: At. Mol. Phys.*, 1986, **19**, 2799; (c) E. van Lenthe, E. J. Baerends and J. G. Snijders, *J. Chem. Phys.*, 1993, **99**, 4597; (d) B. A. Hess, *Phys. Rev. A*, 1986, **33**, 3742.
39. (a) D. A. Pantazis, X.-Y. Chen, C. R. Landis and F. Neese, *J. Chem. Theory Comput.*, 2008, **4**, 908; (b) D. A. Pantazis and F. Neese, *J. Chem. Theory Comput.*, 2009, **5**, 2229.
40. *Chemcraft* http://chemcraftprog.com.

Published on 23 July 2015. Downloaded by University of California - Santa Barbara on 28/07/2015 05:09:18.

Dalton Transactions Accepted Manuscript

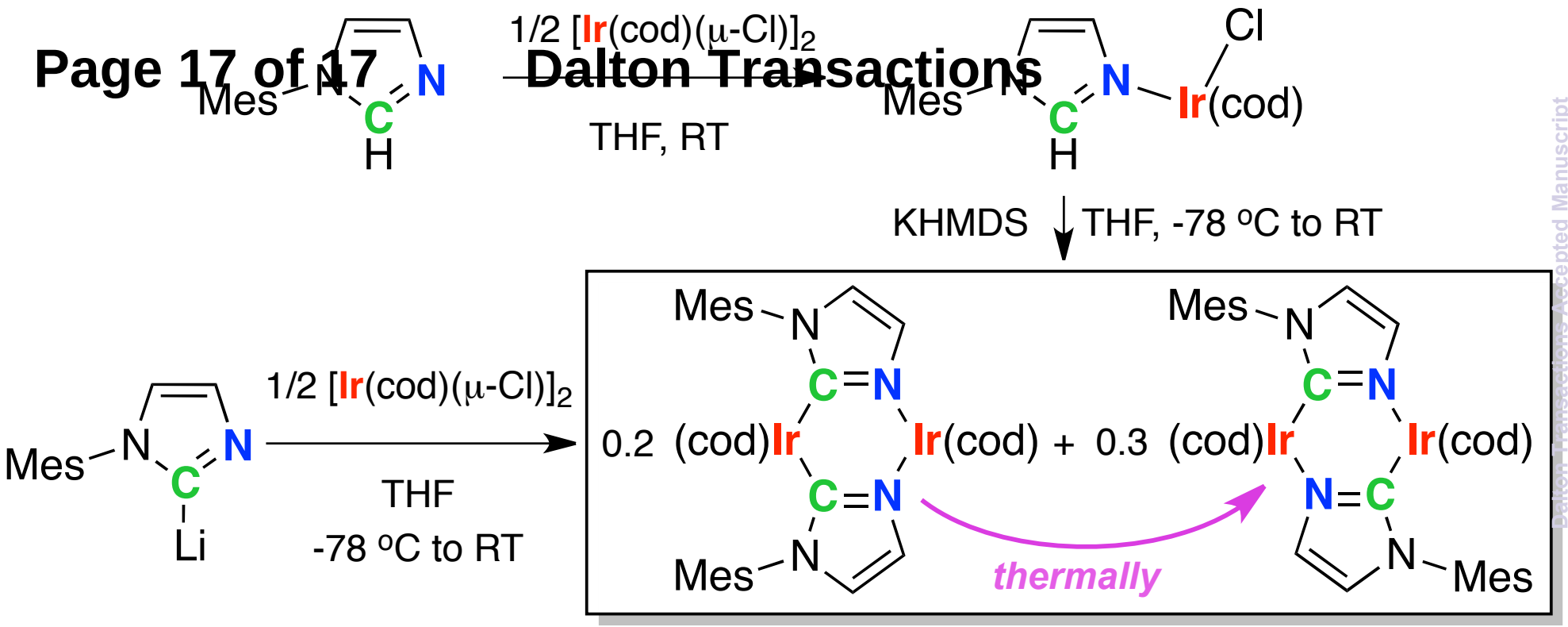

Dalton Transactions Accepted Manuscript